

Krylov Complexity in early universe

Ke-Hong Zhai^{1*} and Lei-Hua Liu^{1†}

Department of Physics, College of Physics,

Mechanical and Electrical Engineering,

Jishou University, Jishou 416000, China

The Lanczos algorithm offers a framework for constructing wave functions in closed and open quantum systems from their Hamiltonians. Since the early universe is inherently an open system, we employ this algorithm to investigate Krylov complexity across various cosmological phases: inflation, radiation domination (RD), and matter domination (MD). Our results highlight a clear distinction in Krylov complexity between the closed- and open-system methodologies. To accurately capture the influence of potentials during RD and MD, we examine a set of inflationary potentials, including the Higgs potential, R^2 inflation, and chaotic inflation, while incorporating violations of slow-roll conditions. This study is conducted in conformal time through the preheating stage. Numerically, we find that the evolution of Krylov complexity and Krylov entropy shows remarkable similarity across different potentials during RD and MD. Furthermore, we rigorously construct an open two-mode squeezed state using the second kind of Meixner polynomial. Based on this construction, we derive for the first time the evolution equations for the squeezing parameter r_k and phase ϕ_k in terms of the scale factor. Our analysis indicates that dissipative effects lead to rapid decoherence-like behavior. In addition, we observe that the inflationary universe behaves as a strongly dissipative system, whereas during the RD and MD epochs the universe exhibits weak dissipative characteristics. This work opens new perspectives for studying the universe from a quantum-informational viewpoint.

*Electronic address: 2023700328@stu.jsu.edu.cn

†Electronic address: liuleihua8899@hotmail.com

Contents

I. Introduction	3
II. Lanczos algorithm with closed-system methodology	6
III. Some setup of early universe	7
A. Inflation, RD and MD	7
B. Various inflationary potentials	9
IV. Evolution of two-mode squeezed state	13
A. Two-mode squeezed state	13
B. The evolution of $r_k(\eta)$ and $\phi_k(\eta)$	14
V. Krylov complexity in closed-system methodology	17
A. Krylov complexity	17
B. Krylov Entropy	19
VI. Krylov complexity with open-system methodology	20
A. Lanczos coefficient and dissipation coefficient	22
1. b_n and μ_2	23
B. General discussion of ϕ_n	25
C. Wave function within open-system methodology	26
D. The power of wave function (83)	30
E. The evolution of $r_k(\eta)$ and $\phi_k(\eta)$ in open-system methodology	30
F. Krylov complexity and Krylov entropy with open-system methodology	31
VII. Summary and outlook	34
Acknowledgements	38
A. The calculation of r_k and ϕ_k within open-system methodology	38
References	41
References	41

I. INTRODUCTION

The concept of complexity has become increasingly important in high-energy physics, although a unified definition is still lacking. Nonetheless, several computational frameworks have been proposed to evaluate it. One major approach is computational complexity, which quantifies the minimum number of logical steps required to perform a given task [1]. Another significant line of research stems from Nielsen and collaborators, who introduced a geometric method for assessing complexity [2–4]. A related framework connects complexity to the Fubini–Study distance in the geometry of information space [5]. However, both geometric approaches depend strongly on the choice of metric on the underlying parameter manifold.

A more recent development is the notion of Krylov complexity, which circumvents the need to construct a parameter manifold altogether [6]. By operating directly in the operator Hilbert space, this approach avoids certain ambiguities inherent in geometric formulations, though the precise connections and distinctions between Krylov complexity and other frameworks remain an active area of research. Within this paradigm, the concept of universal operator growth has been proposed [7], suggesting that the late-time dynamics of quantum operators exhibit universal features encoded in their Krylov complexity. Given a specific quantum operator, one can explicitly compute its Krylov complexity, associated Krylov entropy, and the sequence of Lanczos coefficients using the recursive Lanczos algorithm [6]. The relationship between Krylov complexity and circuit complexity has been examined from contrasting viewpoints: while Ref. [8] argues that the two notions are generally incompatible. However, Ref. [9] shows that, under certain conditions, Krylov complexity is proportional to the distance measured by the Fubini–Study metric.

Recently, Krylov complexity has found broad applications across both condensed matter and high-energy physics. A systematic study employing various orthogonal polynomial bases was carried out in Ref. [10], highlighting the flexibility and robustness of the Krylov framework. Given the central role of the Sachdev–Ye–Kitaev (SYK) model in understanding quantum chaos and holography, Krylov complexity has been actively explored in this context as well [11–13]. Beyond the SYK model, it has been applied to the analysis of generalized coherent states [14], spin systems such as the Ising and Heisenberg models [15–17], and conformal field theories [18–20]. More recently, the formalism has been extended to topological phases of matter [21] and even to quantum field theory [22, 23], underscoring its

growing relevance as a universal diagnostic of operator dynamics and quantum complexity.

It was shown in Ref. [24] that quantum chaos can be interpreted as delocalization in Krylov space, an insight that has reshaped the understanding of operator growth in chaotic systems. Interestingly, exponential growth of Krylov complexity has also been observed in certain integrable models exhibiting saddle-dominated scrambling, with universal features confirmed in Ref. [26]. Since then, the scope of Krylov complexity has continued to expand rapidly. Recent developments include its application to open quantum systems, non-Hermitian dynamics, holography, random matrix theory, and out-of-equilibrium phenomena—see, e.g., Refs. [27–47]. Notably, the framework has also been generalized beyond standard unitary quantum mechanics, with extensions to stochastic dynamics, classical systems, and information-theoretic settings [48].

In this work, we aim to investigate Krylov complexity throughout the entire evolution of the early universe, spanning the inflationary epoch, the subsequent RD era, and the MD era. Previous studies have explored computational complexity during inflation [49–53], uncovering an oscillatory behavior at the onset of inflation and a qualitatively similar pattern in the post-inflationary phase. When quantum effects are incorporated through various quantum-information-theoretic frameworks, the complexity displays irregular oscillations during inflation, a feature that provides a novel diagnostic for distinguishing between competing inflationary models [56].

While several recent works have begun to explore Krylov complexity in the context of the early universe, Ref. [57] stands out as the first to investigate it during inflation, specifically accounting for non-trivial sound speed effects within a closed quantum system framework. However, given that the early universe is more realistically modeled as an open quantum system, interacting with unobservable environmental degrees of freedom, a more physically complete treatment requires going beyond unitary evolution. Addressing this, Ref. [58] adopted an open quantum system approach to study Krylov complexity under a modified dispersion relation during inflation. Their analysis reveals that inflation behaves as a strongly dissipative process, with Krylov complexity displaying a persistent overall increase. A crucial ingredient in this open-system formulation is the explicit construction of the time-evolving wave function, as systematically developed in Ref. [59]. In the present work, we take the wave function derived in Ref. [58] as our starting point to extend the analysis across the full cosmological timeline, from inflation through RD and MD eras.

In previous studies, Krylov complexity has been applied to the early universe using a thermal state as the reference. Refs. [60, 61] extended this framework by incorporating the contribution of the scalar potential—approximated by its quadratic term, and examined the impact of slow-roll violation on complexity growth. In our earlier work [60], the potential was expanded quadratically around its minimum; while analytically convenient, this approximation may not fully capture the dynamics of realistic inflationary scenarios.

It has been suggested by Ref. [65] that many inflationary models are unified into the framework of α -attractors, whose potential form closely resembles that of R^2 inflation. Moreover, Ref. [66] established a connection between the Bunch-Davies vacuum and the two-mode squeezed state. Motivated by these two key insights, we will continue to employ the two-mode squeezed state formalism to study Krylov complexity in the context of the entire early universe. To improve physical fidelity, we plan in upcoming work to generalize the analysis to well-motivated inflationary potentials, including the Higgs potential [62], Starobinsky’s inflation [63], and chaotic inflation [64]. These models encompass most inflationary models and are especially relevant in light of current observational constraints, which strongly favor plateau-like potentials. This extension will allow for a more accurate and observationally grounded exploration of quantum complexity during inflation.

This paper is organized as follows. In Sec. II, we will introduce the Lanczos algorithm. Sec. III will provide a brief review of the early universe, covering inflation, RD, and MD eras, along with three representative inflationary potentials. In Sec. IV, we will present the two-mode squeezed state formalism and numerically solve for the parameter r_k across different cosmological periods. Sec. V will investigate the Krylov complexity in the framework of a closed-system methodology, which Sec. V B will examine the corresponding Krylov entropy. In Sec. VI, we will analyze the Lanczos coefficients and Krylov complexity using an open-system methodology; notably, we will present the evolution equations for ϕ_k and r_k derived within the open two-mode squeezed state formalism in the first time. Finally, conclusions and outlook will be given in Sec. VII.

In this work, we will work in Planck units, namely $c = M_P = G = 1$.

II. LANCZOS ALGORITHM WITH CLOSED-SYSTEM METHODOLOGY

In this section, we will mainly review the Lanczos algorithm with closed-system methodology. First, the operator $\mathcal{O}(t)$ in Heisenberg picture needs to be defined as follows,

$$\partial_t \mathcal{O}(t) = i[H, \mathcal{O}(t)] \quad (1)$$

where H is the Hamiltonian and its solution is

$$\mathcal{O}(t) = e^{iHt} \mathcal{O} e^{-iHt} \quad (2)$$

Next, let's define the Liouvillian super-operator \mathcal{L}_X as $\mathcal{L}_X Y = [X, Y]$, where $[,]$ denotes the commutator. We apply this to Eq. (2), the operator is also expressed as

$$\mathcal{O}(t) = e^{i\mathcal{L}t} \mathcal{O} = \sum_{n=0}^{\infty} \frac{(it)^n}{n!} \mathcal{L}^n \mathcal{O}(0) = \sum_{n=0}^{\infty} \frac{(it)^n}{n!} \tilde{\mathcal{O}}_n \quad (3)$$

where $\mathcal{L}^n \mathcal{O} = \tilde{\mathcal{O}}_n = [H, \tilde{\mathcal{O}}_{n-1}]$ which can serve as the basis for the Hilbert space.

$$\mathcal{O} \equiv |\tilde{\mathcal{O}}\rangle, \mathcal{L}^1 \mathcal{O} \equiv |\tilde{\mathcal{O}}_1\rangle, \mathcal{L}^2 \mathcal{O} \equiv |\tilde{\mathcal{O}}_2\rangle, \mathcal{L}^3 \mathcal{O} \equiv |\tilde{\mathcal{O}}_3\rangle \dots \quad (4)$$

However, they are not orthogonal bases. In order to construct an orthogonal basis, we use the Lanczos algorithm. The first two operators become

$$\mathcal{O}_0 = |\tilde{\mathcal{O}}_0\rangle = \mathcal{O}, \quad |\mathcal{O}_1\rangle = b_1^{-1} \mathcal{L} |\mathcal{O}_0\rangle \quad (5)$$

where $b_1 = \sqrt{(\tilde{\mathcal{O}}_0 \mathcal{L} |\mathcal{L} \tilde{\mathcal{O}}_0\rangle)}$ describing the normalized vector. And the next orthogonal basis is written by

$$|\mathcal{O}_n\rangle = b_n^{-1} |A_n\rangle \quad (6)$$

with

$$|A_n\rangle = \mathcal{L} |\mathcal{O}_{n-1}\rangle - b_{n-1} |\mathcal{O}_{n-2}\rangle, \quad b_n = \sqrt{(A_n | A_n)} \quad (7)$$

where b_n represents the Lanczos coefficients. This iterative relation will stop and produce the finite orthogonal Krylov basis if $b_n = 0$. Subsequently, we express Eq. (3) as follows,

$$\mathcal{O}(t) = e^{i\mathcal{L}t} \mathcal{O} = \sum_{n=0}^{\infty} (i)^n \phi_n(t) |\mathcal{O}_n\rangle \quad (8)$$

where ϕ_n is the wave function satisfying with $\sum_n |\phi_n|^2 = 1$. By substituting Eq. (8) into the Schrödinger equation, we obtain

$$\partial_t \phi_n(t) = b_n \phi_{n-1} - b_{n+1} \phi_{n+1} \quad (9)$$

Next, we define the Krylov complexity using the wave function ϕ_n as follows

$$K = \sum_n n|\phi_n|^2 \quad (10)$$

Additionally, the Lanczos coefficient is bounded via [7],

$$b_n \leq \alpha n + \eta, \quad (11)$$

where α and η encode different information in various models. Note that $b_n = \alpha n + \eta$, which indicates the system is a maximally chaotic dynamical system. For the case of maximal chaos, we obtain the relationship between the Lyapunov exponent and γ and α as follows

$$\lambda = 2\alpha \quad (12)$$

In this work, we will investigate the Krylov complexity for the entire early universe, thus the formula of scale factor $a(\eta)$ should be introduced.

III. SOME SETUP OF EARLY UNIVERSE

In this section, we first review some fundamental aspects of the scale factor in different cosmological epochs. Following the notation of our previous work [60], a central goal of this study is to examine the impact of the inflationary potential on Krylov complexity during the RD and MD eras, particularly due to the violation of slow-roll conditions. The Mukhanov-Sasaki variable incorporates contributions from the potential in a way that does not explicitly reveal its influence on Krylov complexity. Therefore, in this work, we perturb the inflaton field directly. We then introduce several important inflationary potentials: the chaotic inflationary potential, the Starobinsky potential (R^2 inflation), and the Higgs potential. Finally, we employ preheating dynamics to numerically evaluate the effective mass of the inflaton with respect to the scale factor.

A. Inflation, RD and MD

We will follow the notation of [67] to introduce the scale factor. The background metric is the Friedman-Lemaitre-Robertson-Walker (FLRW) metric,

$$ds^2 = a^2(\eta)(-d\eta^2 + d\vec{x}^2), \quad (13)$$

where $a(\eta)$ is the scale factor expressed in conformal time η . Alternatively, the FLRW metric can also be written in terms of physical time t as $ds^2 = -dt^2 + a(t)^2 d\vec{x}^2$, from which the relation $dt = ad\eta$ follows explicitly. Here, we consider a universe dominated by a single component during each epoch, meaning it undergoes successive phases of inflation, RD, and MD. The evolution of the scale factor in each era can be characterized by the equation of state parameter w via

$$w_I = \frac{P_I}{\rho_I}, \quad (14)$$

where P_I and ρ_I are the pressure and energy density, respectively, in each epoch I . To derive the relation between conformal time and the scale factor, we make use of the comoving distance,

$$\chi_{ph}(\eta) = \int_{t_i}^t \frac{dt}{a} = \int_{\ln a_i}^{\ln a} (aH)^{-1} d\ln a \quad (15)$$

where $\chi_{ph}(\eta)$ is the comoving particle horizon distance, and we have used the definition of the Hubble parameter $H = \dot{a}/a$, with $\dot{a} = da/dt$. In terms of the equation of state parameter w_I , the Hubble radius can be expressed as

$$(aH)^{-1} = H_0^{-1} a^{\frac{1}{2}(1+3\omega)} \quad (16)$$

where, for simplicity, we replace ω_I with ω . Integrating Eq. (15) yields an explicit functional relation between the scale factor and the conformal time,

$$\eta = \frac{2H_0^{-1}}{(1+3\omega)} a^{\frac{1}{2}(1+3\omega)}. \quad (17)$$

Consequently, we derive the relation for various time periods

$$\eta = \begin{cases} -(aH_0)^{-1}, & (\omega = -1), \text{ inflation} \\ aH_0^{-1}, & (\omega = \frac{1}{3}), \text{ RD} \\ 2\sqrt{a}H_0^{-1}, & (\omega = 0), \text{ MD} \end{cases} \quad (18)$$

It shows that the various values of ω describe the distinctive periods.

In the following, we outline the fundamental evolution of the universe across its distinct epochs. The universe emerges from a singularity and undergoes a phase of exponential expansion known as inflation. During this period, curvature perturbations transition from quantum to classical after horizon exit, becoming imprinted on the Cosmic Microwave Background (CMB). Subsequently, the universe enters the RD era, characterized by an energy

density $\rho_{\text{rad}}(t) = \rho_{\text{rad}_0}, a_0^4/a(t)^4$, where ρ_{rad_0} and a_0 denote the initial energy density and scale factor at the onset of RD. In this epoch, particles are relativistic. As the temperature drops, particles become increasingly non-relativistic, leading the universe into the MD era, where the energy density evolves as $\rho_{\text{mat}}(t) = \rho_{\text{mat}_0}, a_0^3/a(t)^3$. The transition from RD to MD occurs when the energy densities of radiation and matter equalize. During the subsequent MD epoch, a preheating process can generate particles. We begin by presenting the full action for single-field inflation:

$$S = \int d\eta d^3\vec{x} \sqrt{-g} \left[\frac{1}{2} g^{\mu\nu} \partial_\mu \phi \partial_\nu \phi - V(\phi) \right], \quad (19)$$

where $V(\phi)$ is the potential of inflation. Following the method of [68, 69], the equation of motion for background $\phi(t)$ in RD and MD is

$$\ddot{\phi}(t) + 3H\dot{\phi}(t) + V(\phi)_{,\phi} = 0, \quad (20)$$

where $\ddot{\phi}(t) = \partial_t^2 \phi(t)$, $V(\phi)_{,\phi} = \frac{dV(\phi)}{d\phi}$ and the similar work is found in our previous works [83, 84]. Defining with the effective mass as follows,

$$m_{\text{eff}} = \frac{d^2V}{d\phi^2} = V_{,\phi\phi}. \quad (21)$$

Here, we explain why the effective mass is defined as $m_{\text{eff}} = d^2V/d\phi^2$. For the different inflationary potentials in Eq. (23), we take V_{chaotic} as an example, where one can directly show that $m_{\text{eff}}^2 = m^2$. Based on this, we adopt the same definition of effective mass for all inflationary potentials considered. To solve Eq. (20), we introduce a new variable $\tilde{\phi}(t) = a^{3/2}\phi(t)$, which transforms Eq. (20) into

$$\ddot{\tilde{\phi}}(t) + m_{\text{eff}}^2 \tilde{\phi}(t) = 0, \quad (22)$$

The solution to Eq. (22) is $\phi(t) \propto a^{-3/2} \cos(m_{\text{eff}} t)$, which describes the behavior of $\phi(t)$ during the preheating period. Here, the terms $\frac{9}{4}H^2\tilde{\phi} + \frac{3}{2}\dot{H}\tilde{\phi}$ have been neglected, as they are significantly smaller than the potential contribution. Note that this solution is expressed in physical time t . For the subsequent analysis in this paper, we will transform it into conformal time using $d\eta = dt/a$, as given by Eq. (18).

B. Various inflationary potentials

In this subsection, we will use Eq. (22) to establish a relation between the scale factor and various inflationary potentials. There exist many inflationary models, each characterized by

a distinct potential. Current observational data favor concave potentials [73], a category that includes the potential of R^2 inflation. Furthermore, R^2 inflation remains consistent with observations from inflationary to large scales. From a theoretical perspective, many inflationary models can be unified within the framework of α -attractor models [65], which also encompass R^2 inflation. Motivated by these two considerations, we include R^2 inflation in our analysis. According to the Standard Model, the Higgs field is the only fundamental scalar field in nature; therefore, the Higgs potential serves as another natural choice [62]. Lastly, we consider chaotic inflation with a quadratic potential [64]. Collectively, these choices cover a representative range of inflationary models.

We consider the following inflationary potentials:

$$\left\{ \begin{array}{l} V_{\text{chaotic}} = \frac{1}{2}m^2\phi^2, \\ V_{R^2} = \frac{3}{4}M^2M_p^2(1 - e^{-\sqrt{\frac{2}{3}}\frac{\phi}{M_p}})^2, \\ V_{\text{Higgs}} = \frac{1}{2}m^2\phi^2 + \frac{1}{4}\lambda\phi^4, \end{array} \right. \quad (23)$$

where $M_p = (8\pi G)^{-\frac{1}{2}}$ is the reduced Planck mass. Here, M denotes an energy scale whose value is fixed by the observed amplitude of the primordial power spectrum. Using the solution of Eq. (20) and the relation $dt = ad\eta$, we can express $V_{,\phi\phi}$ as

$$\left\{ \begin{array}{l} V_{\text{chaotic},\phi\phi} = m^2, \\ V_{R^2,\phi\phi} = M^2 \left(-e^{-\sqrt{\frac{2}{3}}\frac{Aa^{-\frac{3}{2}}\sin(m_{\text{eff}}a\eta)}{M_p}} + 2e^{-2\sqrt{\frac{2}{3}}\frac{Aa^{-\frac{3}{2}}\sin(m_{\text{eff}}a\eta)}{M_p}} \right), \\ V_{\text{Higgs},\phi\phi} = m^2 + 3\lambda A^2 a^{-3} \sin^2(m_{\text{eff}}a\eta) \end{array} \right. \quad (24)$$

where $\phi(t) = Aa^{-\frac{3}{2}}\sin(m_{\text{eff}}t)$ and we have used $dt = ad\eta$. The definition of effective mass in Eq. (21) has been employed, and clearly $m_{\text{eff}} = \sqrt{V_{i,\phi\phi}}$ in our work ($i = \text{chaotic}, R^2, \text{Higgs}$). To simplify the subsequent numerical simulations, we define the variable $y = \log_{10} a$. To numerically obtain the effective mass of the distinct inflationary models V_{R^2} and V_{Higgs} , iterative evaluations in terms of $\log_{10} a$ are required, based on Eq. (24). Let us clarify the concept of iterations for the effective mass. The Newton-Raphson method is adopted for its computational efficiency and fast convergence rate. In (24), the effective mass m_{eff} defined by (21) carries the same physical meaning as the left-hand side of (24). Thus, the relation (24) naturally lends itself to an iterative scheme, requiring an initial value m_0 for the effective mass. This value ($m_0^2 = 10^{-12}$) can be fixed by the COBE normalization [74].

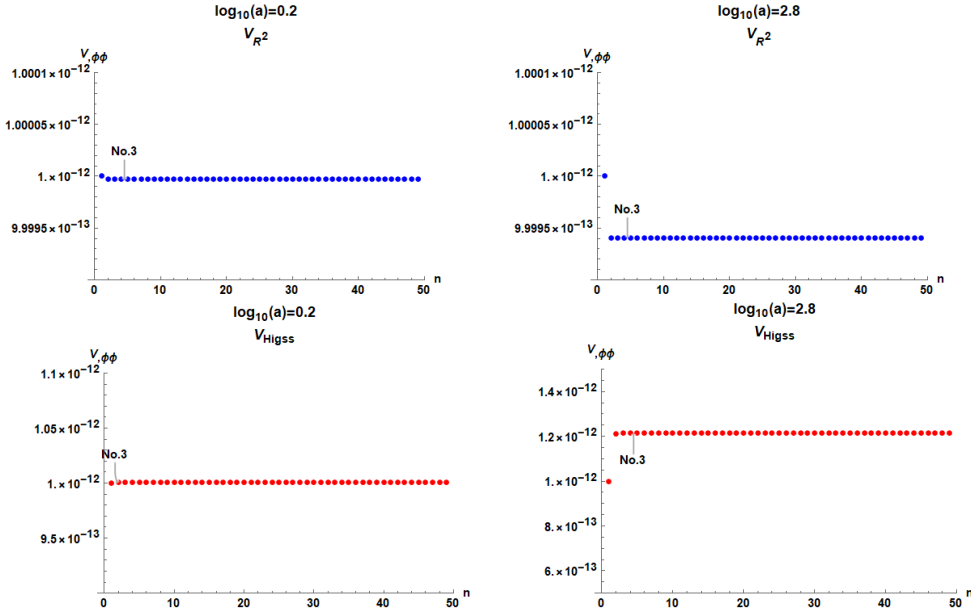


FIG. 1: The numeric of $V_{\phi\phi}$ at first 50 iterations of $V_{R^2,\phi\phi}$ and $V_{\text{Higgs},\phi\phi}$ in $\log_{10} a = 0.2$ and $\log_{10} a = 2.8$, in which we set $M_p = 1$, $m = 10^{-6}$; $M^2 = 10^{-12}$ at V_{R^2} , and $\lambda A^2 = 10^{-4}$ at V_{Higgs} .

In our implementation, we perform 50 iterations for the effective mass, meaning that for each single value of y , the calculation is repeated 50 times.

To check the convergence of $V_{R^2,\phi\phi}$ and $V_{\text{Higgs},\phi\phi}$ within the defined interval, we performed iterations at multiple sampling points from $\log_{10} a = 0$ to $\log_{10} a = 6$ with a step size of 0.05 (this range covers from RD to MD). We find that all points in the range $\log_{10} a = 0$ to $\log_{10} a = 6$ are convergent. As an illustration, Fig. 1 shows the iterative results for $V_{R^2,\phi\phi}$ and $V_{\text{Higgs},\phi\phi}$, where 50 iterations were performed for two specific values of $\log_{10} a$. The parameters used in the figure are chosen as follows: the potential amplitude is constrained by the COBE normalization [74], which bounds its value below 10^{-10} in Planck units, while the inflationary field is a large field with a maximum value around 100 in these units. Consequently, the effective mass for the various potentials is of order 10^{-6} , and all other parameters are set consistently with this scaling.

Let us now discuss the effects of the distinctive parameters of the various potentials. For V_{chaotic} , its effective mass is explicitly set by the inflaton mass, whose value can be fixed via the COBE normalizations. As for V_{R^2} , it contains one parameter M , which acts as the amplitude of the effective mass in Eq. (24); consequently, the range of M is also constrained by the COBE normalization. Finally, the Higgs potential V_{Higgs} involves three parameters:

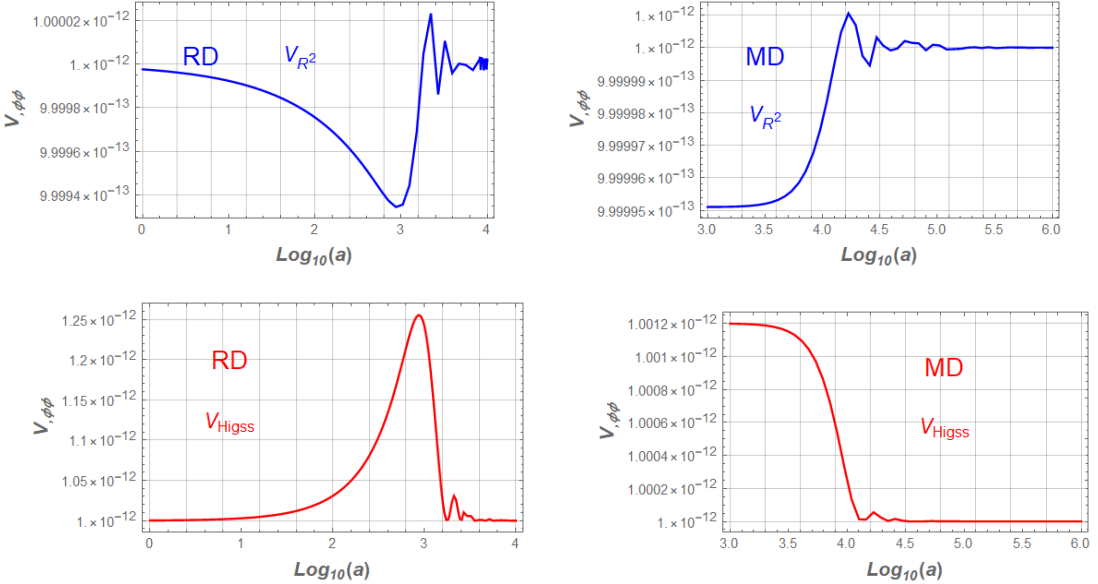


FIG. 2: The numeric of $V_{,\phi\phi}$ in terms of $\log_{10} a$ for potential V_{R^2} , and V_{Higgs} in RD and MD, in which we replace its exact value with the iteration of V_{R^2} , and V_{Higgs} . We set $M_p = 1$, $m = 10^{-6}$; $M^2 = 10^{-12}$ for V_{R^2} , and $\lambda A^2 = 10^{-4}$ for V_{Higgs} .

the Higgs mass m , the coupling constant λ , and the amplitude of the inflaton during pre-heating A . Again, using the COBE normalizations, we can determine the upper bounds on m^2 and λA^2 ; values exceeding these orders would violate the observational constraints. Thus, appropriate parameter values can be set from observational data. As illustrated in Fig. 2, the effective masses for all the considered potentials lie within 10^{-12} in Planck units.

Fig. 2 shows the evolution of $V_{,\phi\phi}$ with respect to $\log_{10} a$ during the RD and MD eras, based on the iterative results for V_{R^2} and V_{Higgs} from Fig. 1. The evolution of the inflationary phase itself is neglected here due to the violation of slow-roll conditions in these periods. From Fig. 2, we observe that the effective mass for R^2 inflation (V_2) decreases during RD and then grows, with oscillations, toward a constant value of approximately 10^{-12} . The behavior for the Higgs potential (V_{Higgs}) is different: it exhibits a peak during RD, after which it decreases and settles into an approximately constant value. Notably, the effective masses for both V_{R^2} and V_{Higgs} are of nearly the same order of magnitude, consistent with the COBE normalization constraint [74].

In this section, we introduce the inflationary, RD, and MD eras, each described by its corresponding scale factor. We also present three representative inflationary potentials that

cover a broad range of model types. An overview of preheating is given, during which the inflaton background oscillates around its potential minimum. Finally, we incorporate this background solution into a numerical evaluation of the effective mass for each of the three potentials.

IV. EVOLUTION OF TWO-MODE SQUEEZED STATE

As we know, the curvature perturbation will become classical as the horizon exits. Ref. [72] already shown the amplification from quantum level to classical level during inflation is naturally a quantum squeezing process. Thus, the two-mode squeezed state is quite a natural choice for investigating the early universe. In this section, we will follow the method of [58] to investigate the evolution of r_k and ϕ_k during inflation, RD and MD.

A. Two-mode squeezed state

First, we will simply recall the two-mode squeezed state. To obtain the two-mode squeezed state, we introduce the unitary operator as follows,

$$\mathcal{U}_k = \hat{\mathcal{S}}_k(\phi_k, r_k) \hat{\mathcal{R}}_k(\theta_k) \quad (25)$$

with

$$\hat{\mathcal{S}}_k = \exp \left[r_k(\eta) \left(e^{-2i\phi_k(\eta)} \hat{c}_{\vec{k}} \hat{c}_{-\vec{k}} - e^{2i\phi_k(\eta)} \hat{c}_{-\vec{k}}^\dagger \hat{c}_{\vec{k}}^\dagger \right) \right] \quad (26)$$

$$\hat{\mathcal{R}}_k(\theta_k) = \exp \left[-i\theta_k(\eta) \left(\hat{c}_{\vec{k}} \hat{c}_{\vec{k}}^\dagger + \hat{c}_{-\vec{k}}^\dagger \hat{c}_{-\vec{k}} \right) \right] \quad (27)$$

where $\hat{\mathcal{S}}_k$ is the squeeze operator and $\hat{\mathcal{R}}_k(\theta_k)$ is the rotation operator, which can be neglected as it only contributes an overall phase factor to the wave function. Applying $\hat{\mathcal{S}}_k(r_k, \phi_k)$ to the vacuum state then yields the wave function of the two-mode squeezed state:

$$|\psi\rangle = \hat{\mathcal{S}}_{\vec{k}}(r_k, \phi_k) |0; 0\rangle_{\vec{k}, -\vec{k}} = \frac{1}{\cosh r_k} \sum_{n=0}^{\infty} (-1)^n e^{2in\phi_k} \tanh^n r_k |n; n\rangle_{\vec{k}, -\vec{k}}. \quad (28)$$

With this wave function, we can now compute the evolution of the squeezed state, which is governed by the parameters r_k and ϕ_k . The derivation of the two-mode squeezed state in Eq. (28) is model-independent, involving only the action of the squeeze operator on the vacuum. Model-specific information is encoded in the parameters r_k and ϕ_k , whose evolution

is determined by the Hamiltonian. This will be confirmed in later sections. Furthermore, the two-mode quantum state $|n; n\rangle_{\vec{k}, -\vec{k}}$ is a Fock state, and its form is given by

$$|n; n\rangle_{\vec{k}, -\vec{k}} = \left[\frac{1}{n!} (c_{\vec{k}}^\dagger c_{-\vec{k}}^\dagger) |0, 0\rangle_{\vec{k}, -\vec{k}} \right], \quad (29)$$

thus, it automatically satisfies both orthogonality and normalization conditions. Here, we need to specify the initial Krylov operator \mathcal{O}_0 in our setup. As mentioned, the wave function is a two-mode squeezed state (28); the initial operator must satisfy the Lanczos algorithm given in Eq. (5). Following Ref. [57], we choose $|\mathcal{O}_0\rangle = |0, 0\rangle_{\vec{k}, -\vec{k}}$ as our initial operator. This choice naturally fulfills the requirements of the Lanczos algorithm, which will be verified in Sec. VI.

B. The evolution of $r_k(\eta)$ and $\phi_k(\eta)$

Numerical simulations of ϕ_k and r_k require their evolution equations, which are derived from the Hamiltonian within the two-mode squeezed state formalism. This work focuses on evaluating the impact of the potential on Krylov complexity. The conventional Mukhanov-Sasaki variable is not ideal for this purpose, as it encapsulates the combined effect of the potential and other factors. To explicitly track the potential's role, we instead perform a direct second-order perturbation of the total action.

$$S = \frac{1}{2} \int d\eta d^3x \left[f'^2 - (\partial_i f)^2 + \left(\frac{a'}{a}\right)^2 f^2 - 2f' f \frac{a'}{a} - a^2 V_{,\phi\phi} f^2 \right] \quad (30)$$

where $f(\eta, \vec{x})$ is the inflaton perturbation defined via $\phi(\eta, \vec{x}) = \bar{\phi}(\eta) + \frac{f(\eta, \vec{x})}{a(\eta)}$, with $\frac{f(\eta, \vec{x})}{a(\eta)} \ll 1$ in Planck units and this perturbation theory will be violated in strong gravitational system. In the current investigations, we focus on the perturbation of inflaton, which is responsible for the formation of large-scale structure; for further details, we refer the reader to [67]. Under the slow-roll condition during inflation, we neglect the potential term, i.e., we assume $\left(\frac{a'}{a}\right)^2 f^2 - 2f' f \frac{a'}{a} \gg a^2 V_{,\phi\phi} f^2$. The Hamiltonian is then constructed as $H = \int d^3x d\eta (\pi f' - \mathcal{L})$, where \mathcal{L} denotes the Lagrangian and π is the conjugate momentum defined by

$$\pi(\eta, \vec{x}) = \frac{\delta L}{\delta f'(\eta, \vec{x})} = f' - \frac{a'}{a} f. \quad (31)$$

According to Eq. (30) and Eq. (31), we obtain

$$H = \frac{1}{2} \int d^3x d\eta [\pi^2 + (\partial_i f)^2 + \frac{a'}{a} (\pi f + f\pi) + a^2 V_{,\phi\phi} f^2]. \quad (32)$$

Using the Fourier decomposition of operator $\hat{f}(\eta, \vec{x})$ and $\hat{\pi}(\eta, \vec{x})$,

$$\hat{f}(\eta, \vec{x}) = \int \frac{d^3k}{(2\pi)^{3/2}} \sqrt{\frac{1}{2k}} (\hat{c}_{\vec{k}}^\dagger f_{\vec{k}}^*(\eta) e^{-i\vec{k}\cdot\vec{x}} + \hat{c}_{\vec{k}} f_{\vec{k}} e^{i\vec{k}\cdot\vec{x}}), \quad (33)$$

$$\hat{\pi}(\eta, \vec{x}) = i \int \frac{d^3k}{(2\pi)^{3/2}} \sqrt{\frac{k}{2}} (\hat{c}_{\vec{k}}^\dagger u_{\vec{k}}^*(\eta) e^{-i\vec{k}\cdot\vec{x}} - \hat{c}_{\vec{k}} u_{\vec{k}} e^{i\vec{k}\cdot\vec{x}}). \quad (34)$$

Substituting equations (33) and (34) into equation (32) to obtain the Hamiltonian operator,

$$\hat{H}_k = (k + \frac{a^2 V_{,\phi\phi}}{2k}) (\hat{c}_{\vec{k}} \hat{c}_{\vec{k}}^\dagger + \hat{c}_{-\vec{k}}^\dagger \hat{c}_{-\vec{k}}) + (\frac{a^2 V_{,\phi\phi}}{2k} + i \frac{a'}{a}) \hat{c}_{-\vec{k}}^\dagger \hat{c}_{\vec{k}}^\dagger + (\frac{a^2 V_{,\phi\phi}}{2k} - i \frac{a'}{a}) \hat{c}_{-\vec{k}} \hat{c}_{\vec{k}}. \quad (35)$$

Based on the Hamiltonian operator and Schrödinger equation

$$i \frac{d}{d\eta} |\psi\rangle = \hat{H}_k |\psi\rangle, \quad (36)$$

we obtain the evolution of equation of r_k and ϕ_k

$$\begin{aligned} r'_k &= \frac{a^2 V_{,\phi\phi}}{2k} \sin 2\phi_k - \frac{a'}{a} \cos 2\phi_k, \\ \phi'_k &= -k - \frac{a^2 V_{,\phi\phi}}{2k} + (\frac{a'}{a} \sin 2\phi_k + \frac{a^2 V_{,\phi\phi}}{2k} \cos 2\phi_k) \coth 2r_k. \end{aligned} \quad (37)$$

In inflation, Eq. (37) will nicely recover into the case of

$$\begin{aligned} r'_k &= -\frac{a'}{a} \cos(2\phi_k), \\ \phi'_k &= -k + \frac{a'}{a} \sin(2\phi_k) \coth(2r_k), \end{aligned} \quad (38)$$

where it is consistent with [52] for $\frac{z'}{z} = \frac{a'}{a}$, since ϵ is constant. Directly solving Eq. (37) numerically is very difficult. Therefore, we introduce the variable transformation $y = \log_{10} a$ and solve Eq. (37) numerically in terms of y ,

$$\begin{aligned} \frac{dr_k}{dy} &= \frac{\ln(10) 10^{\frac{y}{2}(5+3\omega)} V_{,\phi\phi}}{2kH_0} \sin 2\phi_k - \ln(10) \cos 2\phi_k \\ \frac{d\phi_k}{dy} &= -\frac{\ln(10) 10^{\frac{y}{2}(1+3\omega)} k}{H_0} - \frac{\ln(10) 10^{\frac{y}{2}(5+3\omega)} V_{,\phi\phi}}{2kH_0} + \left(\ln(10) \sin 2\phi_k \right. \\ &\quad \left. + \frac{\ln(10) 10^{\frac{y}{2}(5+3\omega)} V_{,\phi\phi}}{2kH_0} \cos 2\phi_k \right) \coth 2r_k \end{aligned} \quad (39)$$

where we have utilized Eq. (17) and $\frac{a'}{a} = H_0 a^{-\frac{1}{2}(1+3\omega)}$.

Before analyzing the figure for r_k , it is important to note that the Krylov complexity depends solely on this quantity. Therefore, in Fig. 3, we show only the numerical results

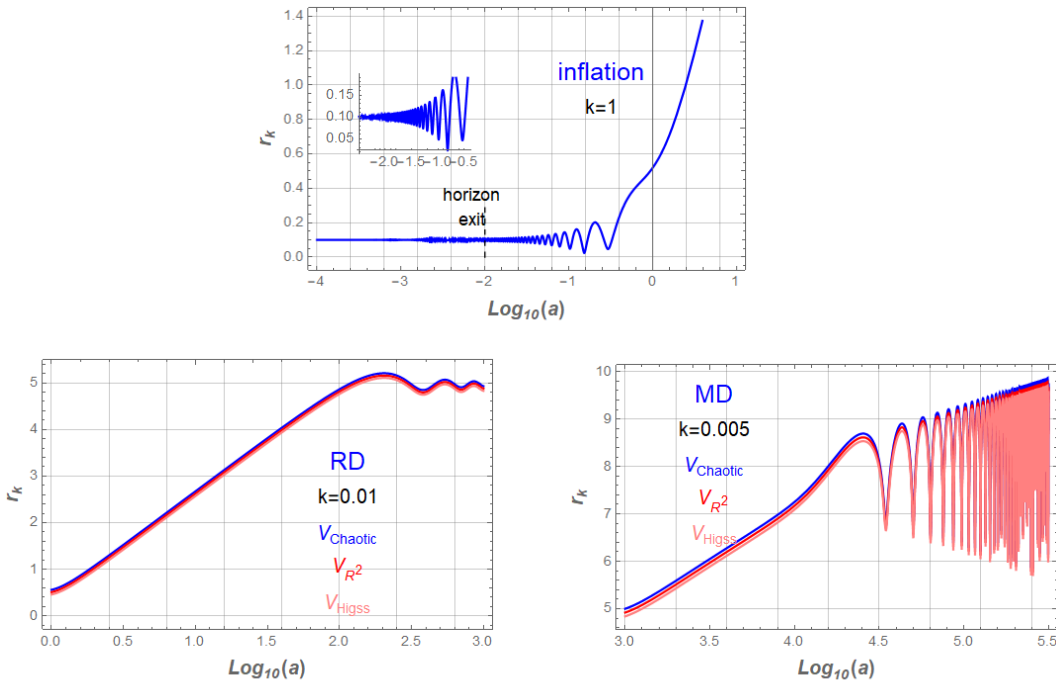


FIG. 3: The numerical solution of r_k in terms of $\log_{10} a$ for three different periods (inflation, RD, and MD), where we set $H_0 = 1$, $k = 1$ in inflation, $k = 0.01$ for RD, $k = 0.005$ for MD. The effect of potential is always ignored in slow-roll inflation. But in RD and MD periods, the impact of potential is taken into account.

for r_k based on Eq. (39). For simplicity, we set $H_0 = 1$ and examine different values of the comoving wavenumber k across various cosmological epochs.

The first panel of Fig. 3 illustrates the evolution of r_k during inflation. Prior to horizon exit, r_k exhibits oscillatory behavior, after which it grows linearly, consistent with the standard result reported in [58]. Following the transition to the RD era, r_k rises and then saturates, fluctuating around a nearly constant value. Notably, different inflationary potentials yield nearly identical trends for r_k , indicating that the specific form of the potential does not significantly influence its evolution.

A similar trend is observed during the MD era, where the behavior of r_k closely resembles that in the RD era. However, we find that the value of the wavenumber k has a pronounced effect: as k decreases, r_k displays increasingly prominent oscillations. We note that presenting results in RD and MD, the contribution of potential is taken into account since the violation of slow roll conditions.

In this section, we have analyzed the evolution of r_k for different inflationary potentials within the single-field inflationary model. Our results indicate that r_k grows during the inflationary epoch. In both the RD and MD eras, r_k exhibits a similar qualitative behavior, saturating and then oscillating around an approximately constant value. Numerical analysis further shows that various inflationary models yield qualitatively similar trends for r_k . Additionally, we find that both the scale factor and the comoving wavenumber significantly influence the evolution of r_k . These features are summarized visually in Fig. 3.

V. KRYLOV COMPLEXITY IN CLOSED-SYSTEM METHODOLOGY

In this section, we conduct numerical simulations of Krylov complexity using the closed-system methodology [54–56]. This framework encompasses both the Krylov complexity and the Krylov entropy. The Krylov complexity is determined by the coefficients r_k and the phases ϕ_k , which are in turn governed by the Hamiltonian operator given in Eq. (35).

A. Krylov complexity

To obtain the Krylov complexity, the key quantity is the wave function. Specifically, the two-mode squeezed state wave function is expressed in the Krylov basis as follows,

$$\mathcal{O}(\eta) = \sum_{n=0}^{\infty} (i)^n \phi_n(\eta) |\mathcal{O}_n\rangle = \frac{1}{\cosh r_k} \sum_{n=0}^{\infty} (-1)^n e^{2in\phi_k} \tanh^n r_k |n; n\rangle_{\vec{k}, -\vec{k}}, \quad (40)$$

where $\mathcal{O}(\eta)$ is the operator of wave function whose original definition can be found in Eq. (8). Then, we find the explicit wave function ϕ_n

$$\phi_n = \frac{1}{\cosh r_k} (-e^{2i\phi_k} \tanh r_k)^n. \quad (41)$$

We define the Krylov complexity in terms of ϕ_n

$$K = \sum_n n |\phi_n|^2 = \cosh^2 r_k \tanh^2 r_k = \sinh^2 r_k. \quad (42)$$

This result explicitly demonstrates the independence of the Krylov complexity from ϕ_k ; hence, only r_k is plotted.

Based on Eq. (42), we show its numerical evolution in Fig. 4, which depicts the behavior of the Krylov complexity throughout the inflationary, RD, and MD eras. Fig. 4 clearly

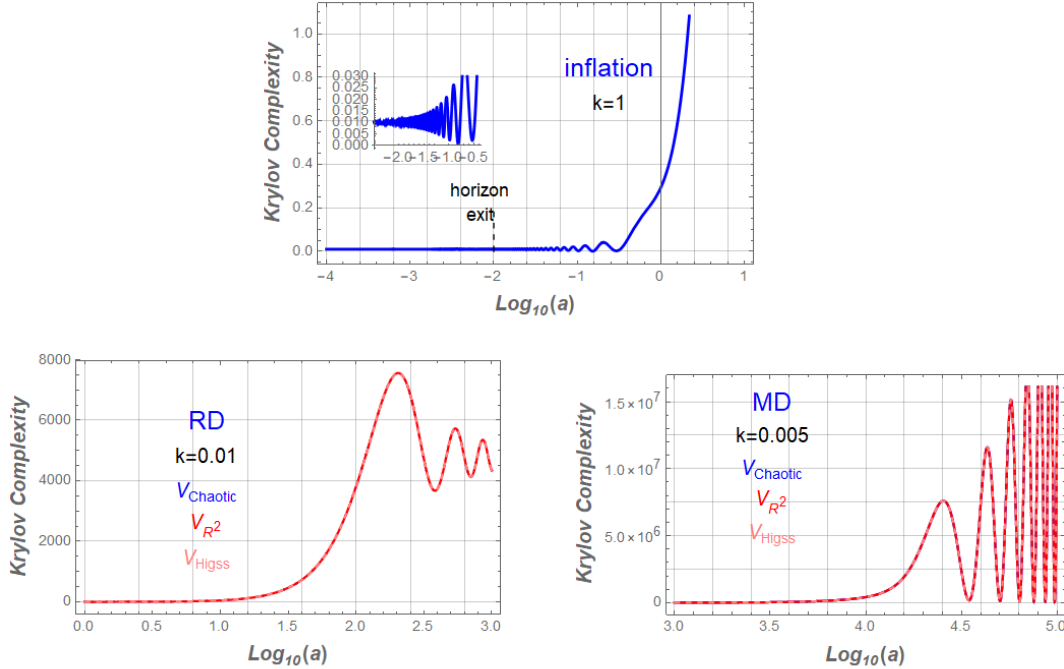


FIG. 4: The numerical of Krylov complexity in terms of $\log_{10} a$ for three different periods (inflation, RD, and MD), where we set $H_0 = 1$, $k = 1$ in inflation, $k = 0.01$ at RD and $k = 0.005$ at MD for simplicity.

reveals a significant growth in the Krylov complexity during the inflationary phase, a result consistent with the modified dispersion case studied in [58]. This finding is also in agreement with related work exploring Krylov complexity under exponential (de Sitter) expansion corresponding to inflation [57]. We note that Ref. [57] identifies the Krylov complexity with the average particle number, which scales proportionally with volume. However, we emphasize that the approach adopted in [57] is specifically applicable to a closed system.

During the RD and MD periods, the Krylov complexity is observed to increase toward certain constant values, around which it subsequently fluctuates. Furthermore, different inflationary models exhibit broadly similar trends in the evolution of Krylov complexity across the respective epochs. Our results are consistent with the analysis in [75], which found that in a closed system the Krylov complexity saturates to approximate constant values even after the scrambling time. The scrambling time itself will be analyzed in the open-system framework, specifically in relation to the Lanczos coefficients, the Lyapunov exponent, among other quantities.

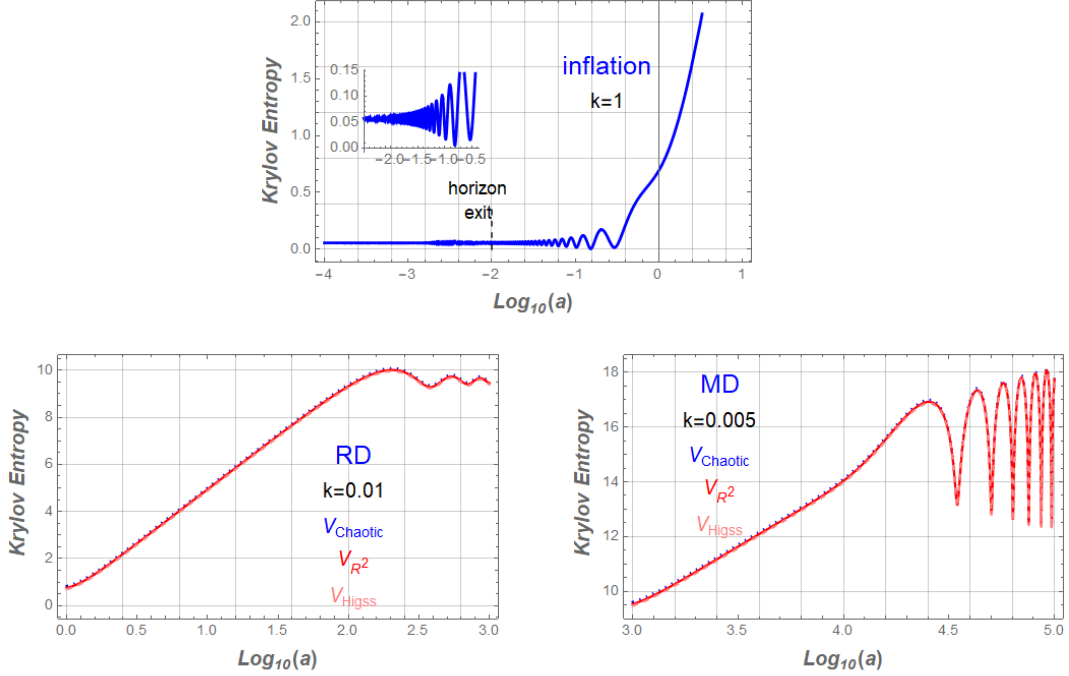


FIG. 5: The numerical of Krylov entropy in terms of $\log_{10} a$ for three different periods (inflation, RD, and MD), where we set $H_0 = 1$, $k = 1$ in inflation, $k = 0.01$ at RD and $k = 0.005$ at MD for simplicity.

B. Krylov Entropy

In quantum systems, entropy is defined as a measure of a system's disorder. The Krylov entropy (K-entropy) serves to quantify the degree of disorder in curvature perturbations. Following [75], the K-entropy is defined as follows,

$$S_K = - \sum_{n=0}^{\infty} |\phi_n|^2 \ln |\phi_n|^2 = \cosh^2 r_k \ln(\cosh^2 r_k) - \sinh^2 r_k \ln(\sinh^2 r_k) \quad (43)$$

where ϕ_n is the wave function (28). Once given the analytic formula of K-entropy, we numerically simulate it in various epochs as shown in Fig. 5.

Fig. 5 illustrates the complete evolutionary profile of the K-entropy across the inflationary, RD, and MD eras, exhibiting a trend similar to that of the Krylov complexity. It can be observed that the curvature perturbations become progressively more disordered during inflation. In the subsequent RD and MD phases, the degree of disorder initially increases before saturating to approximately constant values; nonetheless, the overall trend remains

one of growth, which is closely tied to the evolution of the scale factor. From another perspective, preheating, which generates particles during the MD era, also contributes to the observed increase in the K-entropy.

We now summarize the findings of Section V. In this section, we have conducted a comprehensive analysis of Krylov complexity in the early universe. Our numerical results clearly demonstrate that different inflationary potentials produce nearly identical patterns of evolution for both the Krylov complexity and the K-entropy. Specifically, the Krylov complexity grows during inflation and subsequently saturates to nearly constant values throughout the RD and MD eras. The K-entropy exhibits the same qualitative behavior. To characterize the chaotic features of the early universe more precisely, we must examine the Lanczos coefficients, which, in maximal chaos, play a role analogous to the Lyapunov exponent. These coefficients are identical in form for both the closed- and open-system approaches. In the following, we will employ the open-system methodology to investigate Krylov complexity.

VI. KRYLOV COMPLEXITY WITH OPEN-SYSTEM METHODOLOGY

The preheating process during the MD and RD eras is a highly non-equilibrium phenomenon that generates particles [68, 69]. Furthermore, Ref. [76] demonstrated that the evolution of the universe breaks time-reversal invariance, leading to a violation of energy conservation. For these reasons, the open-system methodology is regarded as more realistic than the closed-system approach. Several open-system methodologies exist for investigating Krylov complexity. Here, we will implement the generalization of the Lanczos algorithm to the Arnoldi iteration via the Heissenberg form [59, 77–79, 81]. Let us review this Arnoldi iteration step by step. We begin by recalling the general Lindblad master equation [80]:

$$\dot{\rho} = -i[H, \rho] + \sum_k [L_k \rho L_k^\dagger - \frac{1}{2} \{L_k^\dagger L_k, \rho\}], \quad (44)$$

where ρ is the density matrix, H is the Hamiltonian, and L_k^\dagger denotes the jump operator (which in our context corresponds to the annihilation operator). Following [81], we consider the open-system dynamics in an infinite-temperature environment. Specifically, we identify the system state ρ with the maximally mixed state (infinite temperature state) ρ_∞ due to the extremal high temperature for the early universe. This assumption defines the inner product for the operator space as $(A, B) = \text{Tr}(\rho_\infty A^\dagger B)$, which is central to our Krylov

complexity calculations. Under this approximation, we obtain

$$\sum_k [L_k \rho_\infty L_k^\dagger - \frac{1}{2} \{L_k^\dagger L_k, \rho_\infty\}] = 0, \quad (45)$$

In this stationary state, it is reasonable to assume that the operator dynamics is governed by

$$\hat{\mathcal{O}}(t) = \exp(i\mathcal{L}t)\hat{\mathcal{O}}, \quad (46)$$

where the Heisenberg-picture Lindbladian \mathcal{L} is given by [59],

$$\mathcal{L} = \mathcal{L}_H + \mathcal{L}_D, \quad \mathcal{L}_H \hat{\mathcal{O}} = [H, \hat{\mathcal{O}}], \quad \mathcal{L}_D = \sum_k [L_k \hat{\mathcal{O}} L_k^\dagger - \frac{1}{2} \{L_k^\dagger L_k, \hat{\mathcal{O}}\}] \quad (47)$$

where \mathcal{L}_H governs the Hermitian dynamics, \mathcal{L}_D denotes the dissipative part, and \mathcal{L} behaves as a superoperator on the operator space. The inner product is defined as $(A|B) := \text{Tr}[\rho_\infty A^\dagger B]$, which explicitly connects the operator space structure to the Krylov basis,

$$\text{span}(\mathcal{O}_0, \dots, \mathcal{O}_n) = \text{span}(\mathcal{V}_0, \dots, \mathcal{V}_n), \quad (48)$$

where \mathcal{V}_n denotes the original Krylov basis, which is generated via the Arnoldi iteration. In this work, we follow the standard construction, beginning with an initial normalized operator $\mathcal{O}_0 \propto \mathcal{O}$. Subsequent Krylov basis vectors are then generated by repeatedly applying the Liouvillian superoperator and performing orthonormalization at each step. To compute the physical quantity, an appropriate basis is required. Following [59], we adopt an orthonormal basis $\{\mathcal{O}_0, \dots, \mathcal{O}_n, \dots\}$ generated by the open-system Lindbladian:

$$\text{span}(\mathcal{O}_0, \dots, \mathcal{O}_n) = \text{span}(\mathcal{V}_0, \dots, \mathcal{V}_n), \quad (49)$$

where \mathcal{V}_n is the original Krylov basis, and we generate this basis by using the Arnoldi iteration, which is started with an initial normalized vector $\mathcal{O}_0 \propto \mathcal{O}$. Thereafter, we construct the subsequent Krylov basis vectors by repeating the following steps:

$$|\mathcal{U}_k) = \mathcal{L}|\mathcal{O}_{k-1}). \quad (50)$$

From $j = 0$ to $n - 1$, we perform the following iterations: 1. $h_{j,k-1} = (\mathcal{O}_j|\mathcal{U}_k)$, 2. $|\tilde{\mathcal{U}}_k) = |\mathcal{U}_k) - \sum_{j=0}^{k-1} h_{j,k-1} |\mathcal{O}_j)$, 3. $h_{k,k-1} = \sqrt{(\tilde{\mathcal{U}}_k|\tilde{\mathcal{U}}_k)}$, it will stop as if $h_{k,k-1} = 0$, otherwise, it is defined as follows,

$$|\mathcal{O}_k) = \frac{|\tilde{\mathcal{U}}_k)}{h_{k,k-1}}. \quad (51)$$

Finally, the Lindbladian can transform into an upper Heissenberg form in the span Krylov basis:

$$\mathcal{L} = \begin{pmatrix} h_{0,0} & h_{0,1} & h_{0,2} & \cdots & \cdots & h_{0,n} \\ h_{1,0} & h_{1,1} & h_{1,2} & \cdots & \cdots & h_{1,n} \\ 0 & h_{2,1} & h_{2,2} & h_{2,3} & \cdots & \cdots \\ \vdots & 0 & h_{3,2} & \cdots & \cdots & \cdots \\ 0 & \vdots & 0 & \vdots & \ddots & h_{n-1,n} \\ 0 & 0 & \vdots & 0 & h_{n,n-1} & h_{n,n} \end{pmatrix} \quad (52)$$

where $h_{m,n} = (\mathcal{O}_m | \mathcal{L} | \mathcal{O}_n)$. As \mathcal{L} is a Hermitian superoperator, the Arnoldi iteration will reduce into the Lanczos algorithm. Following conventions of [58], we represent the generalized Lanczos algorithm as

$$\mathcal{L} | \mathcal{O}_n) = -i c_n | \mathcal{O}_n) + b_{n+1} | \mathcal{O}_{n+1}) + b_n | \mathcal{O}_{n-1}), \quad (53)$$

where the coefficient c_n encodes the information of the open quantum system dynamics for a given Hamiltonian, corresponding to the diagonal elements $h_{n,n}$ in Eq. (52). Meanwhile, the Lanczos coefficients b_n , associated with the off-diagonal elements $h_{n,n-1}$ in Eq. (52), characterize the chaotic behavior of the dynamical system. The orthogonal basis $\mathcal{O}_n = |n, n\rangle_{-\vec{k}, \vec{k}}$ spans the Krylov space defined by Eq. (49). The Liouvillian superoperator \mathcal{L} is equivalent to a Hamiltonian operator that admits a representation in terms of creation and annihilation operators.

A. Lanczos coefficient and dissipation coefficient

Based on the foregoing analysis, we separate the total Hamiltonian (the Lindbladian) into two constituent parts:

$$\mathcal{L}_o = \mathcal{H}_k = \mathcal{H}_{close} + \mathcal{H}_{open} \quad (54)$$

In light of (53), we easily obtain the open part (generating c_n) of Hamiltonian,

$$\mathcal{H}_{open} = (k + \frac{a^2 V_{,\phi\phi}}{2k})(\hat{c}_{-\vec{k}}^\dagger \hat{c}_{-\vec{k}} + \hat{c}_{\vec{k}}^\dagger \hat{c}_{\vec{k}}) \quad (55)$$

and the close part (generating b_n and b_{n-1}) is

$$\mathcal{H}_{close} = (\frac{a^2 V_{,\phi\phi}}{2k} + i \frac{a'}{a}) \hat{c}_{\vec{k}}^\dagger \hat{c}_{-\vec{k}} + (\frac{a^2 V_{,\phi\phi}}{2k} - i \frac{a'}{a}) \hat{c}_{\vec{k}} \hat{c}_{-\vec{k}} \quad (56)$$

where $|\mathcal{O}_n\rangle = |n_{\vec{k}}; n_{-\vec{k}}\rangle$. Specifically, the jump operators L_k appearing in the dissipative term L_D are identified with the annihilation and creation operators in our work, i.e., $L_k = c_k$ and $L_{-k} = c_{-k}^\dagger$. By substituting Eq. (55) and Eq. (56) into Eq. (53), we obtain the equations for c_n and b_n as

$$c_n = i(2n+1)\left(k + \frac{a^2 V_{,\phi\phi}}{2k}\right). \quad (57)$$

$$b_n = n\sqrt{\left[\left(\frac{a^2 V_{,\phi\phi}}{2k}\right)^2 + \left(\frac{a'}{a}\right)^2\right]}. \quad (58)$$

Here, we provide further discussion regarding the coefficients b_n and c_n . In Ref. [81], the coefficient denoted by a_n corresponds to our c_n , and it is also established that c_n is associated with the dissipation coefficient. Meanwhile, we observe that b_n remains identical for both the closed and open systems, as it is determined solely by the Hamiltonian.

In Ref. [7], it is clearly established that the dynamical system is an infinite, chaotic, many-body system as $b_n = \alpha n + \gamma$, where α and γ are parameters that depend on the specific model. In our case, since $b_n \propto n$, the early universe can be regarded as an ideal chaotic system.

1. b_n and μ_2

In this work, we adopt the notation of Ref. [58] to perform numerical simulations of the coefficients b_n and μ_2 . We begin by examining the properties of c_n within our framework. Recall that Eq. (9) (which is essentially the Schrödinger equation) involves only the Lanczos coefficients. The parameter c_n will subsequently appear in the following modified equation:

$$\partial_\eta \phi + 2b_n \partial_n \phi + \tilde{c}_n \phi = 0, \quad (59)$$

Here, we have defined $\tilde{c}_n = -ic_n$. In taking the continuous limit, we have employed the approximations $b_{n+1} \approx b_n$ and $\phi_{n+1} - \phi_{n-1} \approx 2\partial_n \phi$. The coefficients b_n and c_n are defined in Eq. (58) and Eq. (57), respectively. Their general expressions are given by

$$b_n^2 = |1 - \mu_1^2|n(n-1+\beta), \quad c_n = i\mu_2(2n+\beta) \quad (60)$$

where μ_1, μ_2, β are determined by various models and μ_2 plays a role of dissipative coefficient as shown in Ref. [58]. In our work, one can explicitly find $\beta = 1$ and combine Eqs. (57),

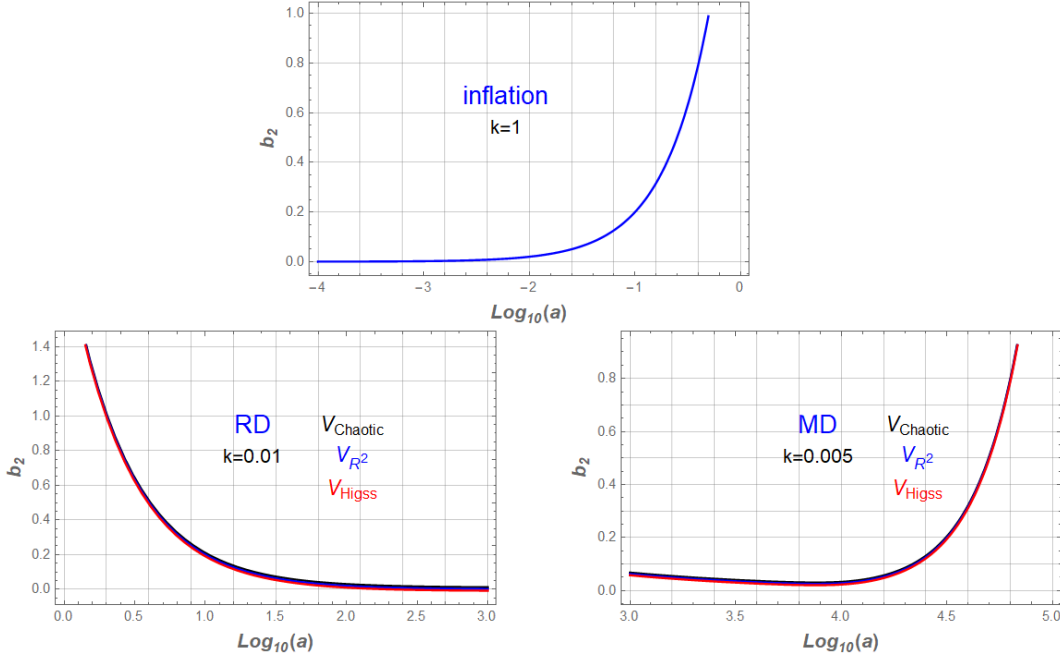


FIG. 6: The plot of $b_n = \lambda$ with $n = 2$. The numerical of b_n in terms of $\log_{10} a$ for three different periods (inflation, RD, and MD), where we set $H_0 = 1$, $k = 1$ in inflation, $k = 0.01$ at RD and $k = 0.005$ at MD for simplicity.

(58), and (60), we find that the parameters μ_1 and μ_2 have the following forms,

$$|1 - \mu_1^2| = \left(\frac{a^2 V_{,\phi\phi}}{2k}\right)^2 + \left(\frac{a'}{a}\right)^2, \mu_2 = k + \frac{a^2 V_{,\phi\phi}}{2k}. \quad (61)$$

It should be noted that during inflation, the parameter μ_2 is primarily determined by the wavenumber k due to the slow-roll conditions. Upon entering the RD and MD eras, which is taking into account the effective mass, we observe that μ_2 becomes smaller than unity, because the effective mass associated with these three types of potentials is much smaller than the momentum k .

We first discuss the Lanczos coefficient b_n . Figure 6 clearly illustrates the three distinct behaviors of b_n during inflation, RD, and MD, where the parameters k and H_0 are set to the same values as in the previous plots. As established in Ref. [59], the Lyapunov exponent λ is related to b_n by $\lambda = 2\alpha$, given the linear form $b_n = \alpha n + \delta$ (with $\delta = 0$ in our case). This explicitly shows that $\lambda = 2\alpha$, or equivalently $\lambda = b_n$ for $n = 2$, as will be demonstrated in Figure 6. Physically, λ characterizes the chaotic nature of the dynamical system. Consequently, in our framework, b_n also reflects the chaotic behavior of the early universe.

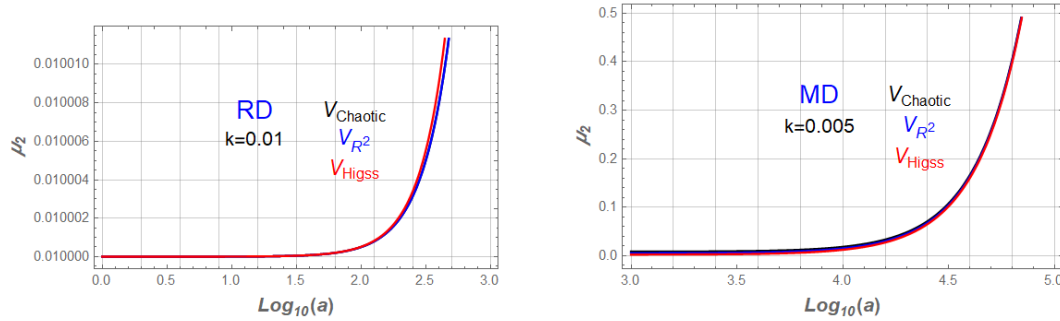


FIG. 7: The numerical of dissipative coefficient μ_2 in terms of $\log_{10} a$ for RD and MD, where we set $H_0 = 1$, $k = 1$ in inflation, $k = 0.01$ at RD and $k = 0.005$ at MD for simplicity. The value of μ_2 indicates the RD and MD are weak dissipative systems.

Figure 6 illustrates the evolution of the coefficient b_n during inflation, RD, and MD. Based on the analysis of b_n , the degree of chaos increases due to the exponential expansion of the background spacetime. As the energy scale decreases, b_n decreases correspondingly with the temperature. During MD, particles are produced via the preheating mechanism known as parametric resonance, leading to an increase in b_n .

Finally, we analyze the dissipation coefficient μ_2 , which is related to c_n , thereby confirming previous results from Ref. [58]. Figure 7 clearly shows the evolution of μ_2 in RD and MD. The value of μ_2 during inflation is not shown in Fig. 7 because $\mu_2 = k = 1$ for the chosen wavenumber k in the inflationary scenario. As asserted in Ref. [58], inflation constitutes a strong dissipative system with $\mu_2 \geq 1$, while RD and MD are weak dissipative systems with $\mu_2 \ll 1$, a result explicitly corroborated by Fig. 7.

To summarize the chaotic features of the early universe: First, chaos is enhanced by the exponential expansion. Then, as the energy scale diminishes, chaos decreases. Finally, the generation of particles during MD through the preheating process increases chaos once again.

B. General discussion of ϕ_n

Before investigating the Krylov complexity, we discuss the general properties of ϕ_n since the definition of Krylov complexity is explicitly represented by $C_K = \sum_{n=1}^{+\infty} n|\phi_n|^2$. We will

follow the general discussion of ϕ_n via Refs. [58, 81]. Eq. (59) is rewritten by

$$\partial_\eta \phi + n(\chi\mu\phi + 2\alpha\partial_n\phi) = 0, \quad (62)$$

where we have defined $\tilde{c}_n = n\chi\mu$ and $b_n = n\alpha$. As η approaches infinity, the solution of Eq. (62) has the form $\phi(n) \propto e^{-n\xi}$ with $\xi = \frac{2\alpha}{\mu\chi}$, where this form will appear in RD or MD due to their weak dissipative nature. In the weak dissipative region, the corresponding Krylov complexity behaves as follows: it increases exponentially at the onset, with the average position given by $C_k \propto e^{2\alpha\eta}$ before reaching η_* . After this point, the Krylov complexity saturates to a constant value ξ when $\eta > \eta_*$, where $\eta_* \sim \frac{1}{2\alpha} \ln \frac{2\alpha}{\chi\mu}$ dubbed as the scrambling time. It is evident that η_* determines the range of exponential growth of Krylov complexity, determined by the dynamical system itself. It is straightforward to demonstrate that $\exp(2a\eta_*) = \xi$. After some simple algebra, we obtain the formula ξ in our case as follows,

$$\xi = \frac{2\sqrt{(\frac{a^2 V_{\phi\phi}}{2k})^2 + (\frac{a'}{a})^2}}{(2 + \frac{1}{n})(k + \frac{a^2 V_{\phi\phi}}{2k})} \quad (63)$$

From this formula, we observe that ξ is not strictly constant; it varies with respect to a and k . Consequently, a significant change in the background will have a substantial impact on Krylov complexity. In this section, we examined the general properties of Krylov complexity without providing the precise formula for ϕ_n . To fully capture the information concerning Krylov complexity within the framework of the open-system methodology, it is essential to have the exact wave function for ϕ_n .

C. Wave function within open-system methodology

Although we constructed the wave function for an open system in reference [58], based on the framework established in [81], this wave function cannot capture the complete information since it is the function of the conformal time η . To clearly illustrate this issue, we will first present our constructed wave function as follows:

$$\phi_n = \frac{\operatorname{sech}\eta}{1 + \mu_2 \tanh\eta} |1 - \mu_1^2|^{\frac{n}{2}} \left(\frac{\tanh\eta}{1 + \mu_2 \tanh\eta} \right)^n. \quad (64)$$

To perform the Taylor expansion around μ_2 to the leading order ($\mu_2 = 0$), we obtain the expression

$$\phi_n \approx \operatorname{sech}(\eta) \tanh^n(\eta) + \mathcal{O}(\mu_2^n).$$

To relate with Eq. (41), we can find one explicit correspondence between r_k and η . To include the parameter of ϕ_k , we will follow the guidelines provided in Appendix D of [7] to rigourisly derive the so-called open two-mode squeezed state, which will accurately reproduce the wave function represented in (41).

For deriving the two-mode squeezed state in open system, we first introduce the concept of orthogonal polynomial sequence (OPS) $\{P_n(x)\}_{n \geq 0}$, it satisfied with the following recurrence relation,

$$P_{n+1}(x) = (x - \tilde{c}_n)P_n(x) - b_n^2 P_{n-1}(x), \quad \text{for } n \geq 1 \quad (65)$$

where x represents the Hamiltonian, \tilde{c}_n is associated with the dissipative coefficient, and b_n refers to the Lanczos coefficient. The sequence begins with the initial conditions $P_0(x) = 1$ and $P_1(x) = x - c_0$. For an open system, we have $P_n(x; \alpha, \eta) = \det(x - \mathcal{L}_n)$, where \mathcal{L}_n is the Hamiltonian for the n -th quantum state. This determinant encodes information about b_n as represented by the corresponding matrix. Based on the definition of L , we express it in terms of x^n or e_n , which will be used to derive the wave function using the open-system methodology.

To obtain the similar recurrence relation as (53), we introduce the the natural orthonormal basis $\{e_n\}$, and meanwhile P_n is represented in terms of e_n

$$P_n(x) = \left(\prod_{k=1}^n b_k \right) e_n, \quad \text{and} \quad x^n = \mathcal{L}^n e_0, \quad (66)$$

where x is the parameter of P_n , \mathcal{L} represents our Hamiltonian expressed in terms of creation and annihilation operators, and $|e_n\rangle \equiv |\mathcal{O}_n\rangle = |n_{\vec{k}}; n_{-\vec{k}}\rangle$. By combining Equation (65) with Equation (66), we derive the following recurrence relation.

$$b_{n+1}e_{n+1} + b_n e_{n-1} = (x - \tilde{c}_n)e_n. \quad (67)$$

Here, x functions as the Hamiltonian. Given the recurrence of P_n , it aligns with the second kind of Meixner polynomials, denoted as $M_n(x; \delta, \eta_1)$. Its generating function is

$$\sum_{n=0}^{\infty} M_n(x; \delta, \eta_1) \frac{t^n}{n!} = ((1 + \delta t)^2 + t^2)^{-\eta_1/2} \exp(x \arctan(\frac{t}{1 + \delta t})) \quad (68)$$

The inverse polynomial of $\{M_n(x; \delta, \eta_1)\}_{n \geq 0}$ is $\{Q_n(x; \delta, \eta_1)\}_{n \geq 0}$, which is defined as

$$Q_n(x) = \sum_{k=0}^n \mu_{n,k} x^k, \quad \text{and} \quad x^n = \sum_{k=0}^n \mu_{n,k} P_k(x). \quad (69)$$

where $\mu_{n,k}$ refers to a triangular linear transform with matrix elements that relate x to P_n . This formula demonstrates that the polynomials P_n is expressed in terms of x . All three orthogonal polynomial sequences (OPS) mentioned are examples of Sheffer orthogonal polynomials, which are defined as a set of polynomials $\{P_n(x)\}_{n \geq 0}$ characterized by a generating function,

$$\sum_{n=0}^{\infty} P_n(x) \frac{t^n}{n!} = f(t) \exp(xg(t)). \quad (70)$$

And the inverse polynomials are give by

$$\sum_{n=0}^{\infty} Q_n(x) \frac{t^n}{n!} = \frac{1}{f(g^{(-1)}(t))} \exp(xg^{(-1)}(t)), \quad (71)$$

where $g^{(-1)}(t)$ stands for the compositional inverse of $g(t)$, which have the following relationship

$$g(g^{(-1)}(t)) = t. \quad (72)$$

Back to the Meixner polynomials of the second kind, we find that

$$f(t) = ((1 + \delta t)^2 + t^2)^{-\eta/2}, \quad \text{and} \quad g(t) = \arctan\left(\frac{t}{1 + \delta t}\right). \quad (73)$$

Our target function is $Q_n(x)$, and the rationale will be provided in the final derivations. To obtain $Q_n(x)$, we need to know the formula for $g^{(-1)}$. The compositional inverse polynomial of $g(t)$ is

$$t = g(g^{(-1)}(t)) = \arctan\left(\frac{g^{(-1)}(t)}{1 + \delta g^{(-1)}(t)}\right), \quad (74)$$

Next,

$$\frac{g^{(-1)}(t)}{1 + \delta g^{(-1)}(t)} = \tan(t) \quad (75)$$

And after a few simple calculations,

$$g^{(-1)}(t) = \frac{\tan(t)}{1 - \delta \tan(t)}, \quad (76)$$

where δ is a parameter determined by various models. Combine Eqs. (76) and (71), we obtain the inverse polynomials of $\{M_n(x; \delta, \eta_1)\}_{n \geq 0}$ as following,

$$\sum_{n=0}^{\infty} Q_n(x) \frac{t^n}{n!} = \frac{\sec(t)^{\eta_1}}{(1 - \delta \tan(t))^{\eta_1}} \exp\left(x \frac{\tan(t)}{1 - \delta \tan(t)}\right). \quad (77)$$

After the changing the variable as $t = i\eta$ and $\delta = i\mu_2$, where η (conformal time) and μ_2 (dissipation coefficient) are our defined parameters. Making use of $\tan i\eta = i \tanh \eta$ and $\cos i\eta = \cosh \eta$, the generating function of the inverse polynomials become

$$\sum_{n=0}^{\infty} Q_n(x) \frac{(i\eta)^n}{n!} = \frac{\operatorname{sech}(\eta)^{\eta_1}}{(1 + \mu_2 \tanh(\eta))^{\eta_1}} \exp\left(x \frac{i \tanh(\eta)}{1 + \mu_2 \tanh(\eta)}\right). \quad (78)$$

Based on Eqs. (66) and (69), we obtain

$$(e_d | \mathcal{L}^n | e_0) = \mu_{n,d} \prod_{k=1}^n b_k. \quad (79)$$

Furthermore, we have

$$(e_d | e^{i\mathcal{L}\eta} | e_0) = \prod_{k=1}^d b_k \sum_{n=0}^{\infty} \frac{(i\eta)^n}{n!} \mu_{n,d}. \quad (80)$$

In light of (69), we obtain

$$\sum_{n=0}^{\infty} \frac{(i\eta)^n}{n!} \mu_{n,d} = \frac{\operatorname{sech}\eta}{1 + \mu_2 \tanh \eta} \frac{1}{d!} \frac{(i \tanh \eta)^d}{(1 + \mu_2 \tanh \eta)^d}, \quad (81)$$

Then we utilize $b_n = \alpha n = \sqrt{|1 - \mu_1^2|} n$ in our case, we naturally get the following formula,

$$(e_n | e^{i\mathcal{L}\eta} | e_0) = \frac{\operatorname{sech}\eta}{1 + \mu_2 \tanh \eta} |1 - \mu_1^2|^{\frac{n}{2}} \frac{(i \tanh \eta)^n}{(1 + \mu_2 \tanh \eta)^n} \quad (82)$$

thus, we obtain the wave function

$$|\mathcal{O}(t)\rangle = e^{i\mathcal{L}\eta} |e_0\rangle = \frac{\operatorname{sech}\eta}{1 + \mu_2 \tanh \eta} \sum_{n=0}^{\infty} |1 - \mu_1^2|^{\frac{n}{2}} \frac{(-1 \exp(2i\phi_k(\eta)) \tanh \eta)^n}{(1 + \mu_2 \tanh \eta)^n} |e_n\rangle$$

where

$$|\mathcal{O}_n\rangle = |e_n\rangle$$

In our calculations, we multiply a phase factor $ie^{2i\phi_k(\eta)}$ which does not alter the wave function. Finally, we set $r_k = \eta$, allowing us to denote the two-mode squeezed state within the open system as,

$$\phi_n(\eta) = (-1)^n e^{2in\phi_k} \frac{\operatorname{sech} r_k}{1 + \mu_2 \tanh r_k} |1 - \mu_1^2|^{\frac{n}{2}} \frac{(\tanh r_k)^n}{(1 + \mu_2 \tanh r_k)^n}. \quad (83)$$

This wave function constitutes the central result of this paper. Its leading-order expansion of ϕ_n in terms of μ_2 is consistent with the wave function presented in (41). The idea of

performing a variable change is inspired by the construction of coherent states, where a key element is the displacement operator, defined as

$$D(\eta) = e^{iHt},$$

with H being the corresponding Hamiltonian, and where the parameter t can be re-expressed in terms of r_k and ϕ_k . As noted in Ref. [9], a generalized coherent state can be derived by constructing a generalized displacement operator based on the appropriate group representation theory.

D. The power of wave function (83)

We discuss the two-mode squeezed state in an open system, as described in equation (83). In contrast to the two-mode squeezed state derived from closed-system methodology, our wave function (83) is more physically realistic, since it includes the contribution of open system via Hamiltonian. Furthermore, although our derivation is obtained within the context of the early universe, this wave function is also widely applicable in fields such as quantum optics, quantum information, and condensed matter physics, where physical information is encoded in the parameters μ_1 and μ_2 , which are determined by the specific system Hamiltonian. Finally, we verify the validity of our results by requiring that the recurrence relation (65), which is equivalent to the Lanczos algorithm, be satisfied. This connection underscores the utility of the Lanczos algorithm, which offers a systematic framework for constructing the wave function directly from the Hamiltonian, even for open quantum systems.

E. The evolution of $r_k(\eta)$ and $\phi_k(\eta)$ in open-system methodology

Following the standard procedure, we derive the evolution equations for r_k and ϕ_k with respect to conformal time η . The details of this derivation are provided in Appendix A. The

resulting evolution is summarized by the following equations:

$$\begin{aligned} r'_k &= \frac{|1 - \mu_1^2|^{\frac{1}{2}} \sinh 2r_k \left(\frac{a^2 V_{,\phi\phi}}{2k} \sin 2\phi_k - \frac{a'}{a} \cos 2\phi_k \right) - \sinh 2r_k \mu'_2}{(\sinh 2r_k + 2\mu_2 \cosh^2 r_k)} \\ \phi'_k &= - \left(k + \frac{a^2 V_{,\phi\phi}}{2k} \right) + \frac{1}{2} \left(\frac{a^2 V_{,\phi\phi}}{2k} \cos 2\phi_k + \frac{a'}{a} \sin 2\phi_k \right) \\ &\quad \left[|1 - \mu_1^2|^{\frac{1}{2}} \frac{\tanh r_k}{1 + \mu_2 \tanh r_k} + |1 - \mu_1^2|^{-\frac{1}{2}} (\tanh^{-1} r_k + \mu_2) \right], \end{aligned} \quad (84)$$

where prime denotes the varying with respect to the conformal time η . We change into the variable $y = \log_{10} a$, the evolution equation of r_k and ϕ_k will become as,

$$\begin{aligned} \frac{H_0}{\ln 10} 10^{-\frac{y}{2}(1+3\omega)} \frac{dr_k}{dy} &= \frac{|1 - \mu_1^2|^{\frac{1}{2}} \sinh 2r_k \left(\frac{10^{2y} V_{,\phi\phi}}{2k} \sin 2\phi_k - H_0 10^{-\frac{y}{2}(1+3\omega)} \cos 2\phi_k \right) - \sinh 2r_k \mu'_2}{(\sinh 2r_k + 2\mu_2 \cosh^2 r_k)} \\ \frac{H_0}{\ln 10} 10^{-\frac{y}{2}(1+3\omega)} \frac{d\phi_k}{dy} &= - \left(k + \frac{10^{2y} V_{,\phi\phi}}{2k} \right) + \frac{1}{2} \left(\frac{10^{2y} V_{,\phi\phi}}{2k} \cos 2\phi_k + H_0 10^{-\frac{y}{2}(1+3\omega)} \sin 2\phi_k \right) \\ &\quad \left[|1 - \mu_1^2|^{\frac{1}{2}} \frac{\tanh r_k}{1 + \mu_2 \tanh r_k} + |1 - \mu_1^2|^{-\frac{1}{2}} (\tanh^{-1} r_k + \mu_2) \right] \end{aligned} \quad (85)$$

where

$$\begin{aligned} \mu_2 &= k + \frac{10^{2y} V_{,\phi\phi}}{2k}, \quad \mu'_2 = H_0 10^{-\frac{y}{2}(1+3\omega)} \frac{10^{2y} V_{,\phi\phi}}{k} + \frac{10^{2y} V'_{,\phi\phi}}{2k} \\ |1 - \mu_1^2| &= \left(\frac{10^{2y} V_{,\phi\phi}}{2k} \right)^2 + (H_0 10^{-\frac{y}{2}(1+3\omega)})^2. \end{aligned}$$

During the calculations, we accounted for the background of ϕ using conformal time η via preheating, as demonstrated by the various potentials in Eq. (24). Consequently, μ_2 and μ_1 also vary with respect to conformal time, since they include contributions from the potential and the scale factor a .

Fig. 8 clearly illustrates the evolution of r_k across various epochs, including inflation, RD, and MD. It is evident that the different potentials produce similar trends for r_k . Unlike in Fig. 3, there is no oscillation of r_k once dissipation effects are considered. Additionally, the trend of r_k varies, particularly during the MD phase, where the evolution consistently shows an increase. These differences will result in distinctive evolutions of Krylov complexity and Krylov entropy.

F. Krylov complexity and Krylov entropy with open-system methodology

In this section, we continue our investigation using the wave function (83) to calculate the Krylov complexity and Krylov entropy. The procedure for these calculations follows

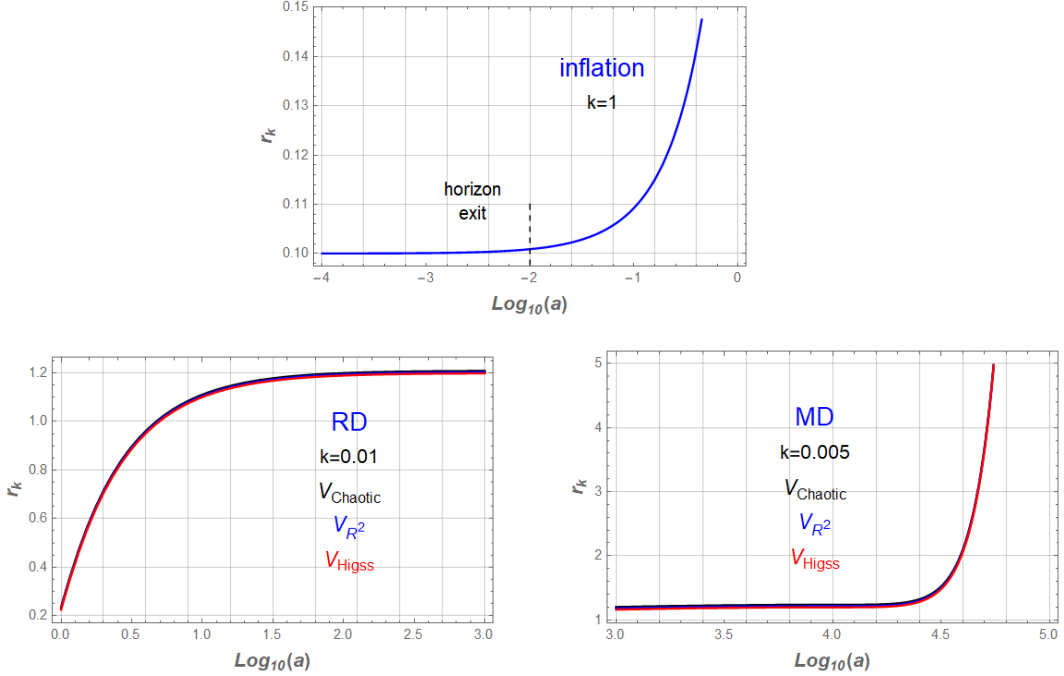


FIG. 8: The numerical of r_k in terms of $\log_{10} a$ for three different periods (inflation, RD, and MD), where we set $H_0 = 1$, $k = 1$ in inflation, $k = 0.01$ at RD and $k = 0.005$ at MD for simplicity.

precisely that of our previous study [58]. The only modification is the substitution of the parameter r_k for η in the formulas for Krylov complexity and Krylov entropy, which are given as follows:

$$K = \frac{\operatorname{sech}^2 r_k |1 - \mu_1^2| \tanh^2 r_k}{[1 + 2\mu_2 \tanh r_k + (\mu_2^2 - |1 - \mu_1^2|) \tanh^2 r_k]^2} \quad (86)$$

and

$$S_k = \frac{\operatorname{sech}^2 r_k}{A^2} [(1 + \mu_2 \tanh r_k)^2 \ln(1 + \mu_2 \tanh r_k)^2 - \tanh^2 r_k |1 - \mu_1^2| \ln \tanh^2 r_k - [(1 + \mu_2 \tanh r_k)^2 - |1 - \mu_1^2| \tanh^2 r_k] \ln \operatorname{sech}^2 r_k - \tanh^2 r_k |1 - \mu_1^2| \ln |1 - \mu_1^2|] \quad (87)$$

where we have defined $A = 1 + 2\mu_2 \tanh r_k + (\mu_2^2 - |1 - \mu_1^2|) \tanh^2 r_k$. It straightforwardly demonstrates the leading order of Krylov complexity (86) and Krylov entropy (87) will reduce to Eq. (42) and Eq. (43) under the weak dissipative approximation, namely, $\mu_2 \ll 1$.

Fig. 9 illustrates the evolution of Krylov complexity during inflation, RD, and MD. During inflation, Krylov complexity exhibits exponential growth, a behavior consistent with the closed-system methodology. In contrast, its evolution in the RD and MD epochs differs significantly with the closed-system methodology as shown in Fig. 4. For the open-system methodology, Krylov complexity in RD shows a decreasing trend, while in MD it first peaks

as the scale factor a increases and subsequently declines to a constant value. Notably, the magnitude of Krylov complexity in the open-system methodology is substantially lower than in the closed-system methodology across both RD and MD.

Our numerical analysis indicates that this suppression originates from the $\text{sech}(r_k)$ term in Eq. (86), an effect presents the dissipation strength. We have shown that both the RD and MD epochs can be approximated as weakly dissipative systems, characterized by $\mu_2 < 1$. Recalling that Krylov complexity quantifies operator growth in a many-body system, and our earlier finding $b_n = \alpha n$ indicates that the universe is fully chaotic, the significantly reduced operator growth observed in the open-system methodology reveals that: dissipation generically leads to a faster suppression of operator growth compared to that in a closed-system methodology.

An understanding of the role of dissipation makes it clear that the magnitude of the Krylov entropy in open-system methodology is lower than that in the closed-system methodology, as demonstrated by a comparison of Figs. 10 and 5. The evolutionary trend is particularly distinct during the RD and MD epochs, as shown in Fig. 10. In RD, the Krylov entropy initially rises to a peak before saturating to a constant value. In MD, it first remains at a nearly constant level before declining and settling at a lower asymptotic value. Overall, both the cosmological background conditions and dissipative effects significantly influence the behavior of Krylov complexity and Krylov entropy.

In this section, we employed the wave function (83) to study the Krylov complexity and Krylov entropy. By comparing our results with those from a closed-system methodology, we observed that dissipative effects not only alter the overall evolution of the system but also suppress the magnitude of both the Krylov complexity and entropy. Since Krylov complexity quantifies operator growth, a fundamental quantum feature of dynamical systems, the suppressed growth in the open-system methodology indicates that dissipation induces more rapid decoherence-like behavior. Furthermore, we note that different inflationary potentials yield nearly identical trends for both Krylov complexity and entropy across the various cosmological epochs.

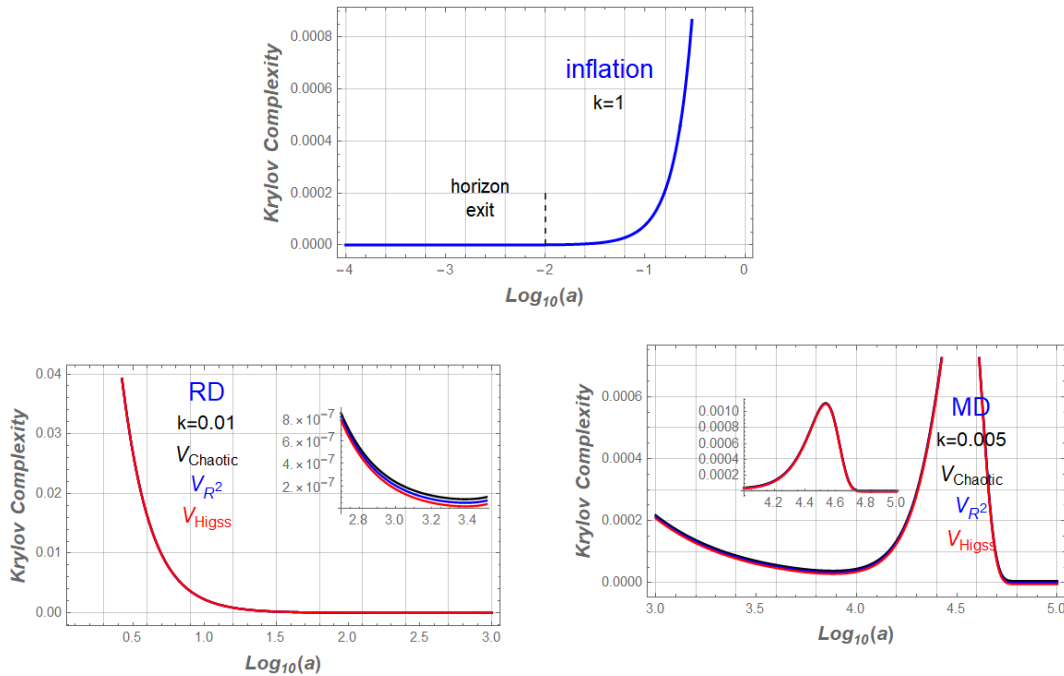


FIG. 9: The numerical of Krylov complexity in terms of $\log_{10} a$ for three different periods (inflation, RD, and MD), where we set $H_0 = 1$, $k = 1$ in inflation, $k = 0.01$ at RD and $k = 0.005$ at MD for simplicity.

VII. SUMMARY AND OUTLOOK

The definition of Krylov complexity is precise and unambiguous, particularly in contrast to the various definitions of circuit complexity. Its uniqueness remove the need to introduce a parametric manifold to conceptualize complexity. Furthermore, Krylov complexity characterizes the growth of operator supported within a dynamical system, and its magnitude indicates the effective quantum size of that system. Krylov complexity is fundamentally based on the Lanczos algorithm, a powerful method for diagnosing the nature of dynamical systems, whether chaotic, integrable, or free. The key diagnostic is the behavior of the Lanczos coefficient b_n , whose asymptotic growth with index n serves as an indicator of the system's dynamical phase. For instance, a linear growth $b_n \sim \alpha n$ is a hallmark of quantum chaos. In our work, we emphasize that the Lanczos coefficient explicitly reveals the early universe as a many-body, infinite, and chaotic system. From a cosmological standpoint, the universe is fundamentally an open system. Notably, the Lanczos algorithm provides a natural framework for constructing the wave function of an open system using the second kind of

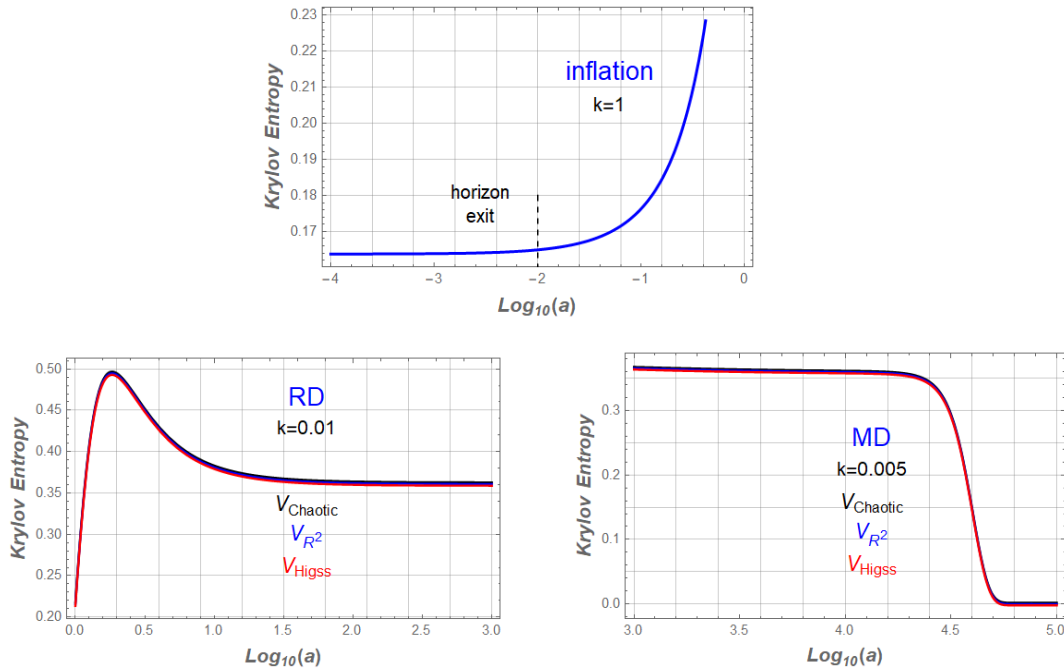


FIG. 10: The numerical of Krylov entropy in terms of $\log_{10} a$ for three different periods (inflation, RD, and MD), where we set $H_0 = 1$, $k = 1$ in inflation, $k = 0.01$ at RD and $k = 0.005$ at MD for simplicity.

Meixner polynomials. Given these insights, it is particularly important to investigate Krylov complexity throughout the evolution of the early universe, encompassing the inflationary, RD, and MD eras.

In this paper, we thoroughly examine Krylov complexity in both open- and closed-system methodologies. Our primary result is the derivation of the two-mode squeezed state using the open-system methodology, along with the calculation of its evolution equations for $\phi_k(\eta)$ and $r_k(\eta)$. Below, we present our key findings.

(a). In Sec. II, we introduce the Lanczos algorithm and the associated Lanczos coefficients, a framework applicable to both open and closed systems. As highlighted in [7], the Liouvillian superoperator effectively acts as a Hamiltonian when expressed in terms of creation and annihilation operators. Our investigation of Krylov complexity spans the entire evolution of the universe, including the inflationary epoch, RD and MD eras, where the slow-roll conditions are violated, the latter necessitating the inclusion of potential energy contributions.

Sec. III examines several representative inflationary potentials, such as the Higgs poten-

tial, the Starobinsky inflationary potential, and chaotic inflationary models. These models collectively cover a broad ranges of inflationary scenarios, unified through the characteristics of α -attractors. To accurately extract the dynamical information encoded in these potentials, we analyze the evolution of the field ϕ relative to the scale factor during preheating, governed by Eq. (22). From this analysis, we compute the effective mass for the various inflationary potentials, as shown in Fig. 2, where our results indicate that how the effective mass varies with respect to scale factor.

(b). Considering the scale factor and various potentials, we investigate Krylov complexity using the closed-system methodology. First, we numerically simulate the parameter r_k for the two-mode squeezed state, as shown in Fig. 3. The results reveal oscillations before horizon exits and then it exponentially grows during inflation, which become enhanced in the RD and MD eras, eventually settling into constant values. Notably, different potentials yield nearly identical trends for r_k . Based on the numerical results for r_k , we also simulate the corresponding Krylov complexity and Krylov entropy, as depicted in Figs. 4 and 5. Both Krylov complexity and entropy exhibit similar trends across the respective epochs. During inflation, we observe exponential growth, consistent with our previous study [58]. In the RD and MD phases, the trends display an initial enhancement followed by saturation to constant values. Moreover, various inflationary models demonstrate nearly identical trends for both Krylov complexity and entropy, confirming the approximation that the effective mass of the inflaton is approximately constant, as indicated in [60].

(c). Within the open-system methodology, we rigorously derive the wave function of an open system using the second kind of Meixner polynomials, dubbed as the open two-mode squeezed state. This wave function is represented in Eq. (83). Throughout this process, we discover that the Lanczos coefficient b_n and the dissipative coefficient μ_2 are precisely determined by the specific Hamiltonian, leading to the conclusion that b_n is identical across both methodologies. Our findings indicate that $b_n = \alpha n$, suggesting that our universe behaves as an entirely chaotic system. Consequently, the Lyapunov index is equivalent to b_n when $n = 2$. Figure 6 illustrates the chaos present across various epochs. During the inflationary period, chaos increases exponentially before diminishing to a certain level, only to rise again due to the preheating process. Additionally, we examine the evolution of the dissipative coefficient in RD and MD. This analysis builds on previous work in Ref. [58], which discusses the strong dissipative nature of the system during inflation. From Fig. 7,

we confirm that the RD and MD systems are weakly dissipative, characterized by $\mu_2 \ll 1$.

Additionally, we derive the evolution of the squeezing parameters r_k and ϕ_k . Their solutions are coupled, as described by Eq. (84), meaning the solution for r_k depends on that for ϕ_k . Using the wave function given in Eq. (83), we compute the Krylov complexity and Krylov entropy, presented in Eqs. (86) and (87). Their leading-order forms are in good agreement with the corresponding formulas derived within the closed-system methodology.

Following the standard procedure, we require the numerical values of r_k in the open-system framework, as shown in Fig. 8. In contrast to the closed-system case, no oscillations in r_k are observed during inflation. The resulting trends for Krylov complexity and Krylov entropy are depicted in Figs. 9 and 10, respectively. Compared to the closed-system results, the magnitudes of both Krylov complexity and entropy are significantly reduced. Recalling that Krylov complexity quantifies operator growth in a dynamical system, a smaller value indicates suppressed operator growth. This suppression reflects a decoherence-like behavior in the context of Krylov complexity once considering the open-system methodology. While we have achieved a comprehensive understanding of Krylov complexity in the early universe, many ideas still remain to be explored. Here, we outline several future directions.

Our investigation begins with Krylov complexity in single-field inflation. A natural extension of this work involves generalizing it to multi-field frameworks [82–85] and to theories of $f(R)$ gravity [86–88]. Such extensions would allow us to explore the influence of field-space geometry and higher-order Ricci curvature terms on Krylov complexity. Our analysis is based on the Hamiltonian given in (35), which is Hermitian and incorporates open-system methodology. In conventional quantum mechanics, open systems are often treated using a Lindbladian master equation [80, 89], typically involving a non-Hermitian effective Hamiltonian. In our present framework, a systematic approach involves expanding the action to higher orders in the Mukhanov-Sasaki variable.

Secondly, our findings demonstrate that in a weakly dissipative system (such as during RD or MD), the behavior of Krylov complexity deviates from the general behavior outlined in Sec. VI B. One plausible explanation for this discrepancy is the neglect of decoherence effects in the curvature perturbations upon horizon exit. As suggested in Ref. [81], decoherence can lead to a saturation phenomenon in circuit complexity. A conceptually similar mechanism may govern Krylov complexity, particularly regarding the influence of decoherence on the structure of the wave function.

Thirdly, having derived the open two-mode squeezed state wave function presented in (83), several promising avenues for further investigation emerge. For instance, this wave function can be used to calculate two-point correlation functions and derive the corresponding power spectrum. Given that its derivation is model-independent, it offers the flexibility to test its validity by applying it within different theoretical models. Conversely, parameters such as μ_1 and μ_2 can be constrained using observational data from the Cosmic Microwave Background (CMB). Furthermore, it is noteworthy that Ref. [57] suggests the potential applicability of the Complexity=Volume (CV) conjecture to Krylov complexity during inflation, although their analysis is confined to a closed system. In contrast, since our universe is fundamentally an open system, our framework provides a distinct opportunity to investigate the validity of the CV conjecture for Krylov complexity within an open-system methodology.

Acknowledgements

LH and KH are funded by NSFC grant NO. 12165009, Hunan Natural Science Foundation NO. 2023JJ30487 and NO. 2022JJ40340.

Appendix A: The calculation of r_k and ϕ_k within open-system methodology

In this appendix, we present the detailed derivations and calculations for the parameters r_k and ϕ_k based on the open two-mode squeezed state,

$$|\psi\rangle = \frac{\operatorname{sech} r_k}{1 + \mu_2 \tanh r_k} \sum_{n=0}^{\infty} (-1)^n |1 - \mu_1|^{\frac{n}{2}} e^{2in\phi_k} \left(\frac{\tanh r_k}{1 + \mu_2 \tanh r_k} \right)^n |n, n\rangle_{\vec{k}, -\vec{k}} \quad (\text{A1})$$

We will write down our Hamiltonian (35) as follows,

$$\hat{H} = \left(k + \frac{a^2 V_{\phi\phi}}{2k} \right) (\hat{c}_{\vec{k}} \hat{c}_{\vec{k}}^\dagger + \hat{c}_{-\vec{k}}^\dagger \hat{c}_{-\vec{k}}) + \left(\frac{a^2 V_{\phi\phi}}{2k} + i \frac{a'}{a} \right) \hat{c}_{-\vec{k}}^\dagger \hat{c}_{\vec{k}}^\dagger + \left(\frac{a^2 V_{\phi\phi}}{2k} - i \frac{a'}{a} \right) \hat{c}_{-\vec{k}} \hat{c}_{\vec{k}} \quad (\text{A2})$$

Starting from the Schrödinger equation $\hat{H}\psi = i\partial_\eta\psi$ (with $\hbar = 1$), we first evaluate its left-hand side as follows.

$$\begin{aligned}
\hat{H}|\psi\rangle &= \frac{\operatorname{sech} r_k}{1 + \mu_2 \tanh r_k} \sum_{n=0}^{\infty} (-1)^n |1 - \mu_1^2|^{\frac{n}{2}} e^{2in\phi_k} \left(\frac{\tanh r_k}{1 + \mu_2 \tanh r_k} \right)^n \left[\left(k + \frac{a^2 V_{,\phi\phi}}{2k} \right) (\hat{c}_{\vec{k}} \hat{c}_{\vec{k}}^\dagger \right. \\
&\quad \left. + \hat{c}_{-\vec{k}}^\dagger \hat{c}_{-\vec{k}}) |n, n\rangle_{\vec{k}, -\vec{k}} + \left(\frac{a^2 V_{,\phi\phi}}{2k} + i\frac{a'}{a} \right) \hat{c}_{-\vec{k}}^\dagger \hat{c}_{\vec{k}}^\dagger |n, n\rangle_{\vec{k}, -\vec{k}} + \left(\frac{a^2 V_{,\phi\phi}}{2k} - i\frac{a'}{a} \right) \hat{c}_{-\vec{k}} \hat{c}_{\vec{k}} |n, n\rangle_{\vec{k}, -\vec{k}} \right] \\
&= \frac{\operatorname{sech} r_k}{1 + \mu_2 \tanh r_k} \sum_{n=0}^{\infty} (-1)^n |1 - \mu_1^2|^{\frac{n}{2}} e^{2in\phi_k} \left(\frac{\tanh r_k}{1 + \mu_2 \tanh r_k} \right)^n \left[\left(k + \frac{a^2 V_{,\phi\phi}}{2k} \right) (2n + 1) \right. \\
&\quad \left. |n, n\rangle_{\vec{k}, -\vec{k}} + \left(\frac{a^2 V_{,\phi\phi}}{2k} + i\frac{a'}{a} \right) (n + 1) |n + 1, n + 1\rangle_{\vec{k}, -\vec{k}} + \left(\frac{a^2 V_{,\phi\phi}}{2k} - i\frac{a'}{a} \right) n |n - 1, n - 1\rangle_{\vec{k}, -\vec{k}} \right] \\
&= \frac{\operatorname{sech} r_k}{1 + \mu_2 \tanh r_k} \left[\left(k + \frac{a^2 V_{,\phi\phi}}{2k} \right) - |1 - \mu_1^2|^{\frac{1}{2}} e^{2i\phi_k} \frac{\tanh r_k}{1 + \mu_2 \tanh r_k} \left(\frac{a^2 V_{,\phi\phi}}{2k} - i\frac{a'}{a} \right) \right] |0, 0\rangle_{\vec{k}, -\vec{k}} \\
&\quad + \frac{\operatorname{sech} r_k}{1 + \mu_2 \tanh r_k} \left[\left(k + \frac{a^2 V_{,\phi\phi}}{2k} \right) - |1 - \mu_1^2|^{\frac{1}{2}} e^{2i\phi_k} \frac{\tanh r_k}{1 + \mu_2 \tanh r_k} \left(\frac{a^2 V_{,\phi\phi}}{2k} - i\frac{a'}{a} \right) \right] \\
&\quad \sum_{n=1}^{\infty} (-1)^n |1 - \mu_1^2|^{\frac{n}{2}} e^{2in\phi_k} \left(\frac{\tanh r_k}{1 + \mu_2 \tanh r_k} \right)^n |n, n\rangle_{\vec{k}, -\vec{k}} + \frac{\operatorname{sech} r_k}{1 + \mu_2 \tanh r_k} \left[\left(2k + \frac{a^2 V_{,\phi\phi}}{k} \right) \right. \\
&\quad \left. - |1 - \mu_1^2|^{\frac{1}{2}} e^{2i\phi_k} \frac{\tanh r_k}{1 + \mu_2 \tanh r_k} \left(\frac{a^2 V_{,\phi\phi}}{2k} - i\frac{a'}{a} \right) - |1 - \mu_1^2|^{-\frac{1}{2}} e^{-2i\phi_k} \left(\frac{\tanh r_k}{1 + \mu_2 \tanh r_k} \right)^{-1} \right. \\
&\quad \left. \left(\frac{a^2 V_{,\phi\phi}}{2k} + i\frac{a'}{a} \right) \right] \sum_{n=1}^{\infty} (-1)^n n |1 - \mu_1^2|^{\frac{n}{2}} e^{2in\phi_k} \left(\frac{\tanh r_k}{1 + \mu_2 \tanh r_k} \right)^n |n, n\rangle_{\vec{k}, -\vec{k}}
\end{aligned} \tag{A3}$$

Then, the right hand side is following as,

$$\begin{aligned}
i \frac{d}{d\eta} |\psi\rangle &= i \frac{d}{d\eta} \left[\frac{\operatorname{sech} r_k}{1 + \mu_2 \tanh r_k} \sum_{n=0}^{\infty} (-1)^n |1 - \mu_1^2|^{\frac{n}{2}} e^{2in\phi_k} \left(\frac{\tanh r_k}{1 + \mu_2 \tanh r_k} \right)^n |n, n\rangle_{\vec{k}, -\vec{k}} \right] \\
&= i \left[-\frac{(\sinh 2r_k + 2\mu_2 \cosh^2 r_k)r'_k + \sinh 2r_k \mu'_2}{2 \cosh^3 r_k (1 + \mu_2 \tanh r_k)^2} \sum_{n=0}^{\infty} (-1)^n |1 - \mu_1^2|^{\frac{n}{2}} e^{2in\phi_k} \left(\frac{\tanh r_k}{1 + \mu_2 \tanh r_k} \right)^n \right. \\
&\quad \left. |n, n\rangle_{\vec{k}, -\vec{k}} \right] + i \left[\frac{\operatorname{sech} r_k}{1 + \mu_2 \tanh r_k} \sum_{n=0}^{\infty} (-1)^n |1 - \mu_1^2|^{\frac{n}{2}} e^{2in\phi_k} \left(\frac{\tanh r_k}{1 + \mu_2 \tanh r_k} \right)^n \right. \\
&\quad \left. [2i\phi'_k + \frac{2r'_k}{\sin 2r_k (1 + \mu_2 \tanh r_k)} + \frac{|1 - \mu_1^2|'}{2|1 - \mu_1^2|} - \frac{\tanh r_k \mu'_2}{1 - \mu_2 \tanh r_k}] |n, n\rangle_{\vec{k}, -\vec{k}} \right] \\
&= -i \frac{(\sinh 2r_k + 2\mu_2 \cosh^2 r_k)r'_k + \sinh 2r_k \mu'_2}{2 \cosh^3 r_k (1 + \mu_2 \tanh r_k)^2} |0, 0\rangle_{\vec{k}, -\vec{k}} \\
&\quad - i \frac{(\sinh 2r_k + 2\mu_2 \cosh^2 r_k)r'_k + \sinh 2r_k \mu'_2}{2 \cosh^3 r_k (1 + \mu_2 \tanh r_k)^2} \sum_{n=1}^{\infty} (-1)^n |1 - \mu_1^2|^{\frac{n}{2}} e^{2in\phi_k} \left(\frac{\tanh r_k}{1 + \mu_2 \tanh r_k} \right)^n \\
&\quad |n, n\rangle_{\vec{k}, -\vec{k}} + \frac{\operatorname{sech} r_k}{1 + \mu_2 \tanh r_k} \left(-2\phi'_k + i \frac{2r'_k}{\sin 2r_k (1 + \mu_2 \tanh r_k)} + i \frac{|1 - \mu_1^2|'}{2|1 - \mu_1^2|} \right. \\
&\quad \left. - i \frac{\tanh r_k \mu'_2}{1 - \mu_2 \tanh r_k} \right) \sum_{n=1}^{\infty} (-1)^n n |1 - \mu_1^2|^{\frac{n}{2}} e^{2in\phi_k} \left(\frac{\tanh r_k}{1 + \mu_2 \tanh r_k} \right)^n |n, n\rangle_{\vec{k}, -\vec{k}}
\end{aligned} \tag{A4}$$

Substituting Eqs. (A3) and (A4) into the Schrödinger equation yields the following simplified form for the open system's squeezed state:

$$\begin{aligned}
A_1 |0, 0\rangle_{\vec{k}, -\vec{k}} &+ A_1 \sum_{n=1}^{\infty} (-1)^n |1 - \mu_1^2|^{\frac{n}{2}} e^{2in\phi_k} \left(\frac{\tanh r_k}{1 + \mu_2 \tanh r_k} \right)^n |n, n\rangle_{\vec{k}, -\vec{k}} \\
&+ A_2 \sum_{n=1}^{\infty} (-1)^n n |1 - \mu_1^2|^{\frac{n}{2}} e^{2in\phi_k} \left(\frac{\tanh r_k}{1 + \mu_2 \tanh r_k} \right)^n |n, n\rangle_{\vec{k}, -\vec{k}} \\
&= B_1 |0, 0\rangle_{\vec{k}, -\vec{k}} + B_1 \sum_{n=1}^{\infty} (-1)^n |1 - \mu_1^2|^{\frac{n}{2}} e^{2in\phi_k} \left(\frac{\tanh r_k}{1 + \mu_2 \tanh r_k} \right)^n |n, n\rangle_{\vec{k}, -\vec{k}} \\
&+ B_2 \sum_{n=1}^{\infty} (-1)^n n |1 - \mu_1^2|^{\frac{n}{2}} e^{2in\phi_k} \left(\frac{\tanh r_k}{1 + \mu_2 \tanh r_k} \right)^n |n, n\rangle_{\vec{k}, -\vec{k}}.
\end{aligned} \tag{A5}$$

Thus, we obtain $A_1 = B_1$ as

$$\begin{aligned}
&-i \frac{(\sinh 2r_k + 2\mu_2 \cosh^2 r_k)r'_k + \sinh 2r_k \mu'_2}{2 \cosh^3 r_k (1 + \mu_2 \tanh r_k)^2} \\
&= \frac{\operatorname{sech} r_k}{1 + \mu_2 \tanh r_k} \left[\left(k + \frac{a^2 V_{,\phi\phi}}{2k} \right) - |1 - \mu_1^2|^{\frac{1}{2}} e^{2i\phi_k} \frac{\tanh r_k}{1 + \mu_2 \tanh r_k} \left(\frac{a^2 V_{,\phi\phi}}{2k} - i \frac{a'}{a} \right) \right],
\end{aligned} \tag{A6}$$

and we're concerned about the imaginary component,

$$\begin{aligned} & -i \frac{(\sinh 2r_k + 2\mu_2 \cosh^2 r_k)r'_k + \sinh 2r_k \mu'_2}{2 \cosh^3 r_k (1 + \mu_2 \tanh r_k)^2} \\ &= -\frac{\operatorname{sech} r_k}{1 + \mu_2 \tanh r_k} \left[|1 - \mu_1^2|^{\frac{1}{2}} \frac{\tanh r_k}{1 + \mu_2 \tanh r_k} \left(\frac{a^2 V_{,\phi\phi}}{2k} \sin 2\phi_k - \frac{a'}{a} \cos 2\phi_k \right) \right]. \end{aligned} \quad (\text{A7})$$

and therefore, we obtain the evolution of r_k as,

$$r'_k = \frac{|1 - \mu_1^2|^{\frac{1}{2}} \sinh 2r_k \left(\frac{a^2 V_{,\phi\phi}}{2k} \sin 2\phi_k - \frac{a'}{a} \cos 2\phi_k \right) - \sinh 2r_k \mu'_2}{(\sinh 2r_k + 2\mu_2 \cosh^2 r_k)}. \quad (\text{A8})$$

The other side, we have $A_2 = B_2$ showing as

$$\begin{aligned} & \frac{\operatorname{sech} r_k}{1 + \mu_2 \tanh r_k} \left[-2\phi'_k + i \frac{2r'_k}{\sin 2r_k (1 + \mu_2 \tanh r_k)} + i \frac{|1 - \mu_1^2|'}{2|1 - \mu_1^2|} - i \frac{\tanh r_k \mu'_2}{1 - \mu_2 \tanh r_k} \right] \\ &= \frac{\operatorname{sech} r_k}{1 + \mu_2 \tanh r_k} \left[\left(2k + \frac{a^2 V_{,\phi\phi}}{k} \right) - |1 - \mu_1^2|^{\frac{1}{2}} e^{2i\phi_k} \frac{\tanh r_k}{1 + \mu_2 \tanh r_k} \left(\frac{a^2 V_{,\phi\phi}}{2k} - i \frac{a'}{a} \right) \right. \\ & \quad \left. - |1 - \mu_1^2|^{-\frac{1}{2}} e^{-2i\phi_k} \left(\frac{\tanh r_k}{1 + \mu_2 \tanh r_k} \right)^{-1} \left(\frac{a^2 V_{,\phi\phi}}{2k} + i \frac{a'}{a} \right) \right], \end{aligned} \quad (\text{A9})$$

the real component reads as,

$$\begin{aligned} & -\frac{2\phi'_k \operatorname{sech} r_k}{1 + \mu_2 \tanh r_k} = \frac{\operatorname{sech} r_k}{1 + \mu_2 \tanh r_k} \left[\left(2k + \frac{a^2 V_{,\phi\phi}}{k} \right) \right. \\ & \quad \left. - \left(\frac{a^2 V_{,\phi\phi}}{2k} \cos 2\phi_k + \frac{a'}{a} \sin 2\phi_k \right) \left(|1 - \mu_1^2|^{\frac{1}{2}} \frac{\tanh r_k}{1 + \mu_2 \tanh r_k} + |1 - \mu_1^2|^{-\frac{1}{2}} (\tanh^{-1} r_k + \mu_2) \right) \right]. \end{aligned} \quad (\text{A10})$$

Finally, we obtain the evolution equation of ϕ_k as follows,

$$\begin{aligned} \phi'_k = & - \left(k + \frac{a^2 V_{,\phi\phi}}{2k} \right) + \frac{1}{2} \left(\frac{a^2 V_{,\phi\phi}}{2k} \cos 2\phi_k + \frac{a'}{a} \sin 2\phi_k \right) \\ & \left[|1 - \mu_1^2|^{\frac{1}{2}} \frac{\tanh r_k}{1 + \mu_2 \tanh r_k} + |1 - \mu_1^2|^{-\frac{1}{2}} (\tanh^{-1} r_k + \mu_2) \right]. \end{aligned} \quad (\text{A11})$$

It can be verified that Eqs. (A8) and (A11) correctly reduce to Eq. (37) in the limit $\mu_1 = \mu_2 = 0$.

References

[1] S. Aaronson, [arXiv:1607.05256 [quant-ph]].

- [2] M. A. Nielsen, Quant. Inf. Comput. **6** (2006) no.3, 213-262 doi:10.26421/QIC6.3-2 [arXiv:quant-ph/0502070 [quant-ph]].
- [3] M. R. Dowling and M. A. Nielsen, Quant. Inf. Comput. **8** (2008) no.10, 0861-0899 doi:10.26421/QIC8.10-1 [arXiv:quant-ph/0701004 [quant-ph]].
- [4] M. A. Nielsen, M. R. Dowling, M. Gu and A. C. Doherty, Science **311** (2006) no.5764, 1133-1135 doi:10.1126/science.1121541 [arXiv:quant-ph/0603161 [quant-ph]].
- [5] S. Chapman, M. P. Heller, H. Marrochio and F. Pastawski, Phys. Rev. Lett. **120** (2018) no.12, 121602 doi:10.1103/PhysRevLett.120.121602 [arXiv:1707.08582 [hep-th]].
- [6] V. S. Viswanath, Gerhard Müller, The recursion method: application to many body dynamics. Vol. 23. Springer Science and Business Media, 1994.
- [7] D. E. Parker, X. Cao, A. Avdoshkin, T. Scaffidi and E. Altman, Phys. Rev. X **9** (2019) no.4, 041017 doi:10.1103/PhysRevX.9.041017 [arXiv:1812.08657 [cond-mat.stat-mech]].
- [8] S. E. Aguilar-Gutierrez and A. Rolph, Phys. Rev. D **109** (2024) no.8, L081701 doi:10.1103/PhysRevD.109.L081701 [arXiv:2311.04093 [hep-th]].
- [9] P. Caputa, J. M. Magan and D. Patramanis, Phys. Rev. Res. **4** (2022) no.1, 013041 doi:10.1103/PhysRevResearch.4.013041 [arXiv:2109.03824 [hep-th]].
- [10] W. Mück and Y. Yang, Nucl. Phys. B **984** (2022), 115948 doi:10.1016/j.nuclphysb.2022.115948 [arXiv:2205.12815 [hep-th]].
- [11] E. Rabinovici, A. Sánchez-Garrido, R. Shir and J. Sonner, JHEP **06** (2021), 062 doi:10.1007/JHEP06(2021)062 [arXiv:2009.01862 [hep-th]].
- [12] S. K. Jian, B. Swingle and Z. Y. Xian, JHEP **03** (2021), 014 doi:10.1007/JHEP03(2021)014 [arXiv:2008.12274 [hep-th]].
- [13] S. He, P. H. C. Lau, Z. Y. Xian and L. Zhao, JHEP **12** (2022), 070 doi:10.1007/JHEP12(2022)070 [arXiv:2209.14936 [hep-th]].
- [14] D. Patramanis, PTEP **2022** (2022) no.6, 063A01 doi:10.1093/ptep/ptac081 [arXiv:2111.03424 [hep-th]].
- [15] X. Cao, J. Phys. A **54** (2021) no.14, 144001 doi:10.1088/1751-8121/abe77c [arXiv:2012.06544 [cond-mat.stat-mech]].
- [16] F. B. Trigueros and C. J. Lin, SciPost Phys. **13** (2022) no.2, 037 doi:10.21468/SciPostPhys.13.2.037 [arXiv:2112.04722 [cond-mat.dis-nn]].
- [17] R. Heveling, J. Wang and J. Gemmer, Phys. Rev. E **106** (2022) no.1, 014152

doi:10.1103/PhysRevE.106.014152 [arXiv:2203.00533 [cond-mat.stat-mech]].

[18] A. Dymarsky and M. Smolkin, Phys. Rev. D **104** (2021) no.8, L081702 doi:10.1103/PhysRevD.104.L081702 [arXiv:2104.09514 [hep-th]].

[19] P. Caputa and S. Datta, JHEP **12** (2021), 188 [erratum: JHEP **09** (2022), 113] doi:10.1007/JHEP12(2021)188 [arXiv:2110.10519 [hep-th]].

[20] A. Kundu, V. Malvimat and R. Sinha, JHEP **09** (2023), 011 doi:10.1007/JHEP09(2023)011 [arXiv:2303.03426 [hep-th]].

[21] P. Caputa and S. Liu, Phys. Rev. B **106** (2022) no.19, 195125 doi:10.1103/PhysRevB.106.195125 [arXiv:2205.05688 [hep-th]].

[22] P. Z. He and H. Q. Zhang, [arXiv:2411.16302 [hep-th]].

[23] P. Z. He and H. Q. Zhang, JHEP **11** (2024), 014 doi:10.1007/JHEP11(2024)014 [arXiv:2407.02756 [hep-th]].

[24] A. Dymarsky and A. Gorsky, Phys. Rev. B **102** (2020) no.8, 085137 doi:10.1103/PhysRevB.102.085137 [arXiv:1912.12227 [cond-mat.stat-mech]].

[25] B. Bhattacharjee, X. Cao, P. Nandy and T. Pathak, JHEP **05** (2022), 174 doi:10.1007/JHEP05(2022)174 [arXiv:2203.03534 [quant-ph]].

[26] K. B. Huh, H. S. Jeong and J. F. Pedraza, [arXiv:2312.12593 [hep-th]].

[27] J. Erdmenger, S. K. Jian and Z. Y. Xian, JHEP **08** (2023), 176 doi:10.1007/JHEP08(2023)176 [arXiv:2303.12151 [hep-th]].

[28] K. Hashimoto, K. Murata, N. Tanahashi and R. Watanabe, JHEP **11** (2023), 040 doi:10.1007/JHEP11(2023)040 [arXiv:2305.16669 [hep-th]].

[29] M. J. Vasli, K. Babaei Velni, M. R. Mohammadi Mozaffar, A. Mollabashi and M. Alishahiha, Eur. Phys. J. C **84** (2024) no.3, 235 doi:10.1140/epjc/s10052-024-12609-9 [arXiv:2307.08307 [hep-th]].

[30] A. Gill, K. Pal, K. Pal and T. Sarkar, Phys. Rev. B **109** (2024) no.10, 104303 doi:10.1103/PhysRevB.109.104303 [arXiv:2311.07892 [quant-ph]].

[31] B. Bhattacharjee, P. Nandy and T. Pathak, JHEP **01** (2024), 094 doi:10.1007/JHEP01(2024)094 [arXiv:2311.00753 [quant-ph]].

[32] K. Adhikari, S. Choudhury and A. Roy, Nucl. Phys. B **993** (2023), 116263 doi:10.1016/j.nuclphysb.2023.116263 [arXiv:2204.02250 [hep-th]].

[33] T. Q. Loc, [arXiv:2402.07980 [hep-th]].

- [34] P. Caputa, H. S. Jeong, S. Liu, J. F. Pedraza and L. C. Qu, [arXiv:2402.09522 [hep-th]].
- [35] R. Basu, A. Ganguly, S. Nath and O. Parrikar, [arXiv:2402.13694 [hep-th]].
- [36] R. Sasaki, [arXiv:2403.06391 [quant-ph]].
- [37] P. Caputa and K. Kutak, [arXiv:2404.07657 [hep-ph]].
- [38] A. Sahu, [arXiv:2404.09464 [quant-ph]].
- [39] B. Bhattacharjee, S. Sur and P. Nandy, *Phys. Rev. B* **106** (2022) no.20, 205150 doi:10.1103/PhysRevB.106.205150 [arXiv:2208.05503 [quant-ph]].
- [40] J. Kim, J. Murugan, J. Olle and D. Rosa, *Phys. Rev. A* **105** (2022) no.1, L010201 doi:10.1103/PhysRevA.105.L010201 [arXiv:2109.05301 [quant-ph]].
- [41] L. Chen, B. Mu, H. Wang and P. Zhang, [arXiv:2404.08207 [quant-ph]].
- [42] B. Bhattacharjee and P. Nandy, [arXiv:2407.07399 [quant-ph]].
- [43] A. Sánchez-Garrido, [arXiv:2407.03866 [hep-th]].
- [44] A. Chattopadhyay, V. Malvimat and A. Mitra, [arXiv:2405.03630 [hep-th]].
- [45] V. Balasubramanian, R. N. Das, J. Erdmenger and Z. Y. Xian, [arXiv:2407.11114 [hep-th]].
- [46] A. Bhattacharya, R. N. Das, B. Dey and J. Erdmenger, *Phys. Rev. B* **110** (2024) no.6, 064320 doi:10.1103/PhysRevB.110.064320 [arXiv:2406.03524 [hep-th]].
- [47] V. Mohan, *JHEP* **11** (2023), 222 doi:10.1007/JHEP11(2023)222 [arXiv:2308.10945 [hep-th]].
- [48] P. Nandy, A. S. Matsoukas-Roubeas, P. Martínez-Azcona, A. Dymarsky and A. del Campo, [arXiv:2405.09628 [quant-ph]].
- [49] S. Choudhury, S. Chowdhury, N. Gupta, A. Mishara, S. P. Selvam, S. Panda, G. D. Pasquino, C. Singha and A. Swain, *Symmetry* **13** (2021) no.7, 1301 doi:10.3390/sym13071301 [arXiv:2012.10234 [hep-th]].
- [50] P. Bhargava, S. Choudhury, S. Chowdhury, A. Mishara, S. P. Selvam, S. Panda and G. D. Pasquino, *SciPost Phys. Core* **4** (2021), 026 doi:10.21468/SciPostPhysCore.4.4.026 [arXiv:2009.03893 [hep-th]].
- [51] J. L. Lehners and J. Quintin, *Phys. Rev. D* **103** (2021) no.6, 063527 doi:10.1103/PhysRevD.103.063527 [arXiv:2012.04911 [hep-th]].
- [52] A. Bhattacharyya, S. Das, S. Shajidul Haque and B. Underwood, *Phys. Rev. D* **101** (2020) no.10, 106020 doi:10.1103/PhysRevD.101.106020 [arXiv:2001.08664 [hep-th]].
- [53] K. Adhikari, S. Choudhury, H. N. Pandya and R. Srivastava, *Symmetry* **15** (2023) no.3, 664 doi:10.3390/sym15030664 [arXiv:2108.10334 [gr-qc]].

[54] L. H. Liu and A. C. Li, *Phys. Dark Univ.* **37** (2022), 101123 doi:10.1016/j.dark.2022.101123 [arXiv:2102.12014 [gr-qc]].

[55] A. c. Li, X. F. Li, D. f. Zeng and L. H. Liu, *Phys. Dark Univ.* **43** (2024), 101422 doi:10.1016/j.dark.2024.101422 [arXiv:2102.12939 [gr-qc]].

[56] T. Li and L. H. Liu, [arXiv:2309.01595 [gr-qc]].

[57] K. Adhikari and S. Choudhury, *Fortsch. Phys.* **70** (2022) no.12, 2200126 doi:10.1002/prop.202200126 [arXiv:2203.14330 [hep-th]].

[58] T. Li and L. H. Liu, *JHEP* **04** (2024), 123 doi:10.1007/JHEP04(2024)123 [arXiv:2401.09307 [hep-th]].

[59] A. Bhattacharya, P. Nandy, P. P. Nath and H. Sahu, *JHEP* **12** (2022), 081 doi:10.1007/JHEP12(2022)081 [arXiv:2207.05347 [quant-ph]].

[60] T. Li and L. H. Liu, [arXiv:2408.03293 [hep-th]].

[61] T. Li and L. H. Liu, [arXiv:2405.01433 [hep-th]].

[62] P. W. Higgs, *Phys. Rev. Lett.* **13** (1964), 508-509 doi:10.1103/PhysRevLett.13.508

[63] A. A. Starobinsky, *Phys. Lett. B* **91** (1980), 99-102 doi:10.1016/0370-2693(80)90670-X

[64] A. D. Linde, *Phys. Lett. B* **129** (1983), 177-181 doi:10.1016/0370-2693(83)90837-7

[65] M. Galante, R. Kallosh, A. Linde and D. Roest, *Phys. Rev. Lett.* **114** (2015) no.14, 141302 doi:10.1103/PhysRevLett.114.141302 [arXiv:1412.3797 [hep-th]].

[66] A. Albrecht, P. Ferreira, M. Joyce and T. Prokopec, *Phys. Rev. D* **50** (1994), 4807-4820 doi:10.1103/PhysRevD.50.4807 [arXiv:astro-ph/9303001 [astro-ph]].

[67] D. Baumann, doi:10.1142/9789814327183_0010 [arXiv:0907.5424 [hep-th]].

[68] L. Kofman, A. D. Linde and A. A. Starobinsky, *Phys. Rev. D* **56** (1997), 3258-3295 doi:10.1103/PhysRevD.56.3258 [arXiv:hep-ph/9704452 [hep-ph]].

[69] Y. Shtanov, J. H. Traschen and R. H. Brandenberger, *Phys. Rev. D* **51** (1995), 5438-5455 doi:10.1103/PhysRevD.51.5438 [arXiv:hep-ph/9407247 [hep-ph]].

[70] L. H. Liu and W. L. Xu, *Chin. Phys. C* **44** (2020) no.8, 085103 doi:10.1088/1674-1137/44/8/085103 [arXiv:1911.10542 [astro-ph.CO]].

[71] L. H. Liu, *Chin. Phys. C* **47** (2023) no.1, 015105 doi:10.1088/1674-1137/ac9d28 [arXiv:2107.07310 [astro-ph.CO]].

[72] L. P. Grishchuk and Y. V. Sidorov, *Phys. Rev. D* **42** (1990), 3413-3421 doi:10.1103/PhysRevD.42.3413

- [73] Y. Akrami *et al.* [Planck], *Astron. Astrophys.* **641** (2020), A10 doi:10.1051/0004-6361/201833887 [arXiv:1807.06211 [astro-ph.CO]].
- [74] P. A. R. Ade *et al.* [Planck], *Astron. Astrophys.* **594** (2016), A20 doi:10.1051/0004-6361/201525898 [arXiv:1502.02114 [astro-ph.CO]].
- [75] J. L. F. Barbón, E. Rabinovici, R. Shir and R. Sinha, *JHEP* **10** (2019), 264 doi:10.1007/JHEP10(2019)264 [arXiv:1907.05393 [hep-th]].
- [76] C. Cheung, P. Creminelli, A. L. Fitzpatrick, J. Kaplan and L. Senatore, *JHEP* **03** (2008), 014 doi:10.1088/1126-6708/2008/03/014 [arXiv:0709.0293 [hep-th]].
- [77] C. Liu, H. Tang and H. Zhai, *Phys. Rev. Res.* **5** (2023) no.3, 033085 doi:10.1103/PhysRevResearch.5.033085 [arXiv:2207.13603 [cond-mat.str-el]].
- [78] A. A. Nizami and A. W. Shrestha, *Phys. Rev. E* **108** (2023) no.5, 5 doi:10.1103/PhysRevE.108.054222 [arXiv:2305.00256 [quant-ph]].
- [79] P. Nandy, A. S. Matsoukas-Roubeas, P. Martínez-Azcona, A. Dymarsky and A. del Campo, *Phys. Rept.* **1125-1128** (2025), 1-82 doi:10.1016/j.physrep.2025.05.001 [arXiv:2405.09628 [quant-ph]].
- [80] G. Lindblad, *Commun. Math. Phys.* **48** (1976), 119 doi:10.1007/BF01608499
- [81] B. Bhattacharjee, X. Cao, P. Nandy and T. Pathak, *JHEP* **03** (2023), 054 doi:10.1007/JHEP03(2023)054 [arXiv:2212.06180 [quant-ph]].
- [82] L. H. Liu and T. Prokopec, *JCAP* **06** (2021), 033 doi:10.1088/1475-7516/2021/06/033 [arXiv:2005.11069 [astro-ph.CO]].
- [83] L. H. Liu and W. L. Xu, *Chin. Phys. C* **44** (2020) no.8, 085103 doi:10.1088/1674-1137/44/8/085103 [arXiv:1911.10542 [astro-ph.CO]].
- [84] L. H. Liu, *Chin. Phys. C* **47** (2023) no.1, 015105 doi:10.1088/1674-1137/ac9d28 [arXiv:2107.07310 [astro-ph.CO]].
- [85] X. z. Zhang, L. h. Liu and T. Qiu, *Phys. Rev. D* **107** (2023) no.4, 043510 doi:10.1103/PhysRevD.107.043510 [arXiv:2207.07873 [hep-th]].
- [86] L. H. Liu, T. Prokopec and A. A. Starobinsky, *Phys. Rev. D* **98** (2018) no.4, 043505 doi:10.1103/PhysRevD.98.043505 [arXiv:1806.05407 [gr-qc]].
- [87] L. H. Liu, B. Liang, Y. C. Zhou, X. D. Liu, W. L. Xu and A. C. Li, *Phys. Rev. D* **103** (2021) no.6, 063515 doi:10.1103/PhysRevD.103.063515 [arXiv:2007.08278 [astro-ph.CO]].
- [88] L. H. Liu, doi:10.1007/s10773-018-3809-0 [arXiv:1807.00666 [gr-qc]].

- [89] V. Gorini, A. Kossakowski and E. C. G. Sudarshan, *J. Math. Phys.* **17** (1976), 821
doi:10.1063/1.522979
- [90] A. Bhattacharyya, T. Hanif, S. S. Haque and A. Paul, *Phys. Rev. D* **107** (2023) no.10, 106007
doi:10.1103/PhysRevD.107.106007 [arXiv:2210.09268 [hep-th]].